CSIRO PUBLISHING

Australian Journal of Physics

Volume 53, 2000
© CSIRO Australia 2000

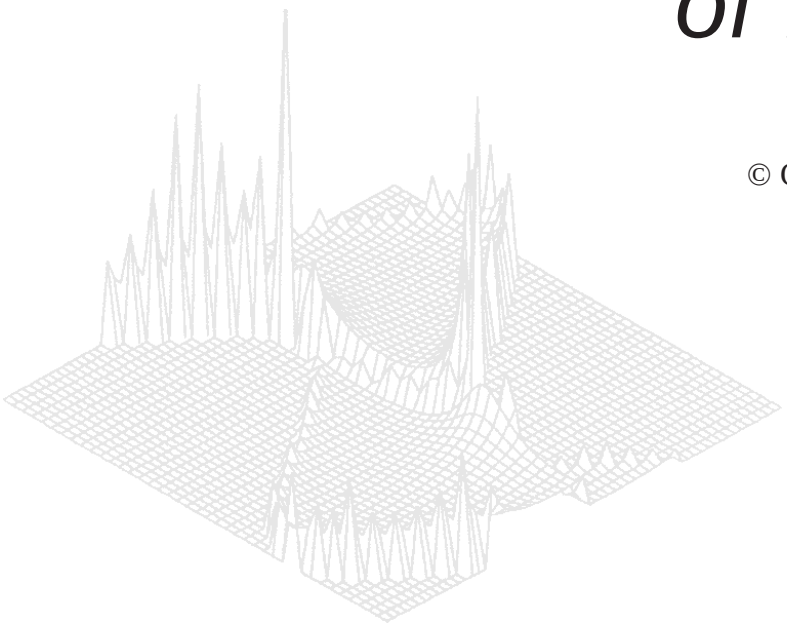

A journal for the publication of
original research in all branches of physics

www.publish.csiro.au/journals/ajp

All enquiries and manuscripts should be directed to
Australian Journal of Physics
CSIRO PUBLISHING
PO Box 1139 (150 Oxford St)
Collingwood Telephone: 61 3 9662 7626
Vic. 3066 Facsimile: 61 3 9662 7611
Australia Email: peter.robertson@publish.csiro.au

Published by **CSIRO** PUBLISHING
for CSIRO Australia and
the Australian Academy of Science

Aust. J. Phys., 2000, **53**, 259–287

Hybrid Model for Drift Waves in Fully Three-dimensional Plasmas: Theory and Applications

J. L. V. Lewandowski

Department of Theoretical Physics, RSPhySE,
Australian National University, Canberra, ACT 0200, Australia.
Present address: Plasma Physics Laboratory,
Institute of Advanced Studies, Princeton University,
Princeton, NJ 08543, USA.

Abstract

A novel fluid/gyro-kinetic hybrid model to study drift waves in low-pressure stellarator plasmas is presented. The ion population is modeled with the collisionless gyro-kinetic equation and the electron population is described using fluid equations. The model equations are written in straight-field-line coordinates and are valid for any magnetic configuration with closed, nested magnetic surfaces. The geometrical effects which enter the final eigenmode equations are derived and discussed in some detail. The numerical method used to solve the coupled, time-dependent, along-the-field-line equations is described. The geometrical effects are discussed in some detail. Numerical calculations are carried out for a three-field period toroidal heliac with small global magnetic shear.

1. Introduction

It is now generally accepted in the fusion community that even if fast, large-scale magnetohydrodynamic (MHD) instabilities can be suppressed, magnetically-confined plasmas always contain sufficient free energy to drive slow, short-scale instabilities. These slow, short-scale instabilities, often called microinstabilities (Liewer 1985), are a major concern as far as confinement is concerned. The cross-field (perpendicular) transport associated with microinstabilities is often one to two orders magnitude larger than the neoclassical transport, and it is called 'anomalous' for this reason (Horton 1984; Manheimer and Lashmore-Davies 1989). In toroidal plasmas, the expansion energy associated with density and temperature gradients is a major source of free energy available to drive microinstabilities (Horton 1989). When the particle distributions display strong departure from Maxwellian distributions, an additional source of free energy is present. When the particle distributions are strongly non-Maxwellian in character, a kinetic theory is required to correctly model microinstability dynamics. This is also true when trapped particle effects are retained in the model.

Substantial efforts have been made to understand microinstability dynamics and the associated transport in tokamak geometry. However, very little work has been published on microinstabilities in stellarator geometry. The earlier work of Bhattacharjee *et al.* (1983) considered an electron drift wave model (with cold ions) in helically symmetric configurations; the main conclusion of the paper by Bhattacharjee *et al.* is that localised and extended modes can coexist in such

© CSIRO 2000 10.1071/PH98111 0004-9506/00/020259$10.00

configurations. The spectrum of the model used by Bhattacharjee *et al.* has been calculated by Persson *et al.* (1996). The first drift wave calculations in realistic stellarator geometry were carried out by Dominguez and co-workers (1992) for the dissipative trapped electron mode (DTEM); they showed that extended modes as well as strongly localised modes do exist (in the linear approximation) in a fully three-dimensional (3d) configuration. The electron drift wave model (with cold ions) in helically symmetric configuration considered by Bhattacharjee *et al.* (1983) and Persson *et al.* (1996) was also studied by Waltz and Boozer (1993). In their paper, Waltz and Boozer pointed out that the local magnetic shear (Lewandowski and Persson 1995, 1996) (and not the global shear) is the key parameter for microturbulence in stellarators (Persson and Lewandowski 1997). All the above-mentioned papers have assumed $T_\mathrm{i} \mapsto 0$ (cold ion approximation). In this paper, we present a hybrid model with finite T_i and a drift-resistive model for the electron population in general 3d confinement devices such as stellarators.

A careful study of microinstabilities in 3d geometries, such as the stellarator configuration, is of crucial importance. In particular, the difference in scalings between the stellarator and tokamak configurations can be, perhaps, attributed to the magnetic topology of these configurations. This paper is part of an ongoing project concerned with drift waves in three-dimensional geometry such as stellarators and tokamaks with field coil ripples.

In view of the complicated (fully 3d) magnetic field geometry of stellarators, most of the published work on drift waves has been done using the so-called $i\delta$ model (Bhattacharjee *et al.* 1983; Waltz and Boozer 1993; Persson *et al.* 1996; Persson and Lewandowski 1997). This model retains important features of electron drift waves (such as curvature drive, parallel ion motion, etc.), while neglecting effects due to particle trapping, finite ion temperature, Landau damping, etc. In the ballooning representation, a single eigenmode equation for the fluctuating electrostatic potential is obtained in which an *ad hoc* parameter, $i\delta$, models the processes which prevent the electron population from reaching a Boltzmann distribution. The electron drift wave is unstable when δ is positive. In a high-density, low-T_e, collisional plasma, a self-consistent correction $i\delta$ can be obtained from a perturbation analysis (Lewandowski 1997*a*). Calculations of collisional drift waves in realistic stellarator geometry have been reported recently. Using two-fluid equations, Lewandowski (1997*b*) studied collisional drift waves in a low-shear stellarator. It was shown that the eigenfunctions for fluctuating quantities (plasma density, electrostatic potential, electron temperature) display a strong ballooning character. The numerically-computed scaling of the linear growth rate as a function of the electron-temperature-gradient parameter η_e was also reported (Lewandowski 1997*b*). The inclusion of finite parallel ion motion in the above model, neglected in Lewandowski (1997*b*), showed that the linear growth rate is reduced, while the $k_\perp$ spectrum of the drift waves was shown to be strongly peaked (Lewandowski 1997*c*). The effect of finite ion temperature was entirely neglected in Lewandowski (1997*a*, *b*, *c*). The limit $T_\mathrm{i}/T_\mathrm{e} \mapsto 0$ is often adopted for the sake of simplicity; however, for realistic plasma discharges, one has to consider $T_\mathrm{i}/T_\mathrm{e} = \mathcal{O}(1)$.

The standard approach to the problem of drift waves is to separate the slow, drift-type modes into two classes depending on the direction of propagation of the mode (electron branch or ion branch); for instance, the dissipative trapped-electron

mode (DTEM) rotates in the electron diamagnetic drift frequency, whereas the ion temperature gradient-driven (ITG) mode rotates in the ion diamagnetic direction. For ITG modes, the usual assumption is to neglect the non-adiabatic part of the density response, which is equivalent to taking the limit $\delta \mapsto 0$ in

$$\widetilde{n} \equiv \frac{\delta n}{n_0} = (1 - i\delta)\widetilde{\Phi}\,. \tag{1}$$

Here δn (n_0) is the perturbed (equilibrium) density and $\widetilde{\Phi} \equiv e\Phi/T_\mathrm{e}$ is the normalised electrostatic potential. In a real plasma, however, the limit $\delta = 0$ is never actually fullfilled; there are always (collisional and collisionless) phenomena which prevent the density response from reaching *perfect* adiabaticity.

One question arises when developing drift wave models for 3d (asymmetric) plasmas: since the physics governing drift waves is the same in tokamak and stellarator plasmas, are there factors which can differentiate, in the *linear* approximation, these two configurations? In view of the complicated (fully 3d) magnetic field geometry of stellarators, the answer to this question is not trivial. Studies of resistive drift waves in a stellarator have shown that the mode structure has, like in tokamak geometry, a ballooning character (Lewandowski 1997*b*, 1997*c*). In a low-shear stellarator, a vanishing radial mode number yields, like in the tokamak case, the fastest linear growth rate (Lewandowski 1998). However, the variation of ∇B along the magnetic field line (weak in the tokamak case, but strong in the stellarator case) has been suggested recently (Lewandowski 1998) as a good candidate to explain the difference in (linear) scaling between tokamaks and stellarators.

There are basically two different approaches to the problem of drift waves. One possible approach is to use (standard) fluid equations (Braginskii 1965) or reduced fluid equations (Drake and Antonsen 1984). The second approach relies on kinetic or gyro-kinetic models (Rutherford and Frieman 1968). Fluid models are generally more tractable mathematically, but they miss important kinetic effects.

In this paper, we present calculations of the ion collisionless gyro-kinetic equation in the linear regime for a low-β stellarator plasma. For simplicity, we neglect the effects of trapped particles. Braginskii's (1965) fluid equations are used to determine the electron dynamics. The perturbed ion density is obtained by a direct integration over velocity space of the ion distribution function, while the perturbed electron density is determined from the electron continuity equation. The closure relation for the perturbed electrostatic potential is the quasineutrality condition. We use the ballooning representation (Connor *et al.* 1978, 1979; Antonsen and Lane 1980) for fluctuating quantities and the equations are written in straight-field-line coordinates (Haeseleer *et al.* 1991). Our initial-value code is convenient for studying the ITG-driven mode in general 3d plasmas (Rudakov and Sagdeev 1961). Since the model presented here is valid for fully 3d (non-axisymmetric) plasmas, it can be applied to stellarator configurations as well as tokamaks with field coil ripple effects.

This paper is organised as follows. In Section 2, we briefly review progress in the ITG mode theory. We pay special attention to the toroidal branch (essentially tokamak geometry) of this mode. In Section 3 we discuss the assumptions made

to obtain our model; the collisionless ion gyro-kinetic equation is written in a form convenient for numerical work and, finally, the quasineutrality condition is derived. In Section 4, a fluid model for the electron dynamics is presented. The numerical method used to solve the time-dependent coupled equations is outlined in Section 5. Numerical results for the toroidal heliac H1-NF (Hamberger *et al.* 1990) are given in Section 6, followed by concluding remarks in Section 7.

2. Toroidal ITG Mode

Since very little work on the ion-temperature-gradient mode in *stellarator* geometry has been done, the aim of this section is to briefly review the tokamak-specific results.

The ITG-driven mode is a drift-type instability which arises from the free energy stored in the ion pressure gradient. In slab geometry and for a flat density profile, the mode is attributed to the coupling between the electron drift wave and the ion acoustic waves. The ITG mode was discovered by Rudakov and Sagdeev (1961). These authors considered a simple model in slab geometry and for a flat density profile, neglecting kinetic effects. The inclusion of magnetic shear and kinetic effects were investigated by Pogutse (1967). Using a fluid model and assuming an adiabatic response for the electrons, a systematic study of the mode structure of the ITG mode, in sheared slab geometry, was carried out by Coppi and co-workers (1967) and others (Antonsen *et al.* 1979; Hassam *et al.* 1990).

As shown by Coppi *et al.* (1967) and by Horton *et al.* (1980), the ITG mode in toroidal geometry is mainly driven by unfavourable magnetic curvature rather than the coupling of the electron drift wave to the ion acoustic waves. It is worth noting that other pressure-gradient-driven modes, such as the collisionless trapped-particle mode (Kadomstev and Pogutse 1971), the trapped-electron mode (Coppi and Mazzucato 1974), and the residual trapped-ion mode (Tang *et al.* 1977), can be driven unstable in the presence of unfavourable magnetic curvature.

Since the ion pressure is a source of free energy that can drive the mode, the linear growth rate depends on the radial density scale length L_n, and the radial ion temperature scale length $L_{T\mathrm{i}}$. In toroidal geometry, the growth rate also depends on the toroidicity parameter, $\epsilon_n \equiv L_n/\bar{R}$, the safety factor q, and the global magnetic shear, $\hat{s} \equiv rdq/dr/q$. For a peaked density profile, the η_i mode can be driven unstable when $\eta_\mathrm{i} \equiv L_n/L_{T\mathrm{i}}$ exceeds a threshold value η_{ic}. The threshold value η_{ic} is typically of the order of unity. In the weak density limit ($1/L_n = 0$), the relevant parameter governing this mode is $L_{T\mathrm{i}}/R$ (Tang *et al.* 1986).

Many authors have considered a fluid approach in order to determine the threshold η_{ic} (Guzdar *et al.* 1983; Jarmen *et al.* 1987; Dominguez and Waltz 1988; Shukla 1990). However, fluid models have the fundamental problem that, for $\eta_\mathrm{i} \sim \eta_{\mathrm{ic}}$, the fluid approximation is not valid since the mode is affected both by magnetic drift and Landau resonances. These fluid models usually assume that the effect of the parallel dynamics is to localise the eigenfunction in the bad curvature region, while the effect on the threshold is small. A more accurate treatment requires a kinetic theory. However, some fluid models (Jarmen *et al.* 1987) can provide a fairly accurate picture of the ITG and η_i modes in some specific regimes. Furthermore, fluid models are mathematically more tractable

than kinetic models. In particular, the *nonlinear* dynamics can be studied with fluid models (Nordman *et al.* 1990; Horton *et al.* 1980; Waltz 1988; Hong and Horton 1990; Guzdar *et al.* 1991; Drake *et al.* 1991; Hamaguchi and Horton 1990, 1992; Kim *et al.* 1991). New fluid equations which retain kinetic effects, the gyro-Landau fluid equations, have been recently developed (Hammett and Perkins 1990; Waltz *et al.* 1992; Hedrick and Leboeuf 1992). These models are in good agreement with fully kinetic models (Parker *et al.* 1994; Dorland and Hammett 1993).

Most of the papers dealing with the kinetic $\eta_{\rm i}$ and ITG modes use a simple geometry of a tokamak with circular, concentric magnetic surfaces. The work of Rewoldt and Tang (1990) is the notable exception. Using an integral kinetic equation, Dong and co-workers (1992) presented a systematic study of the effects of toroidicity, safety factor, global magnetic shear and ion-to-electron temperature ratio, $\tau \equiv T_{\rm i}/T_{\rm e}$. The authors showed that, for moderate shear and $\epsilon_n = 0{\cdot}2$, the maximum growth rate peaks around $k_\theta \rho_s \simeq 0{\cdot}5$, where $k_\theta = nq/r$ and ρ_s is the ion thermal gyro-radius evaluated at the electron temperature. The growth rate is maximised for $\epsilon_n \simeq 0{\cdot}2$, while other parameters are kept fixed. Numerical calculations show that the maximum growth rate is obtained for moderate global magnetic shear, $\hat{s} \simeq 0{\cdot}5$. The mode rotates in the ion direction with a real frequency which becomes more negative as $k_\theta \rho_s$ increases.

The electron dynamics also modifies the ITG and $\eta_{\rm i}$ modes. In the flat density limit, the effect of trapped electron dynamics on these modes is small (Romanelli and Briguglio 1990). As the parameter $\eta_{\rm i}$ increases, it has been shown by Rewoldt and Tang (1990) that the dominant electrostatic instability evolves from the trapped electron mode to the ITG mode. For low electron collisions, the mode rotates in the electron direction; as the electron collision frequency increases, the real part of the frequency decreases, vanishes and ultimately becomes negative (ion direction) (Rewoldt and Tang 1990). Fluid models, such as the one by Nilsson and Weiland (1994), can also be used to retain the effects of trapped electrons.

The trapped ions can also alter the mode (Biglari *et al.* 1989; Dong *et al.* 1992; Xu and Rosenbluth 1991*a*, 1991*b*). In particular, a detailed study of the $\eta_{\rm i}$ mode in tokamak geometry, including an accurate Fokker–Planck collision operator for ion–ion collisions, has been carried out by Xu and Rosenbluth (1991*a*). These authors showed that one important consequence of the effects of ion–ion collisions is the stabilisation of the long-wavelength part of the spectrum. This is an important result because long-wavelength instabilities can produce large cross-field transport.

As discussed in the beginning of this section, it is important to treat finite Larmor radius (FLR) effects and kinetic effects, such as Landau damping, accurately. We therefore use the ion gyro-kinetic equation to study the $\eta_{\rm i}$ mode in stellarator geometry. As a first approximation, we neglect the ion trapping and ion–ion collisions. As we shall see below, the neglect of these effects drastically simplifies the solution of the gyro-kinetic equation. Collisional and trapping effects can be retained in the model; the code developed by Kotschenreuther *et al.* (1988, 1992) for tokamak geometry takes into account such effects.

3. Ion Dynamics

In this section, we describe the ion collisionless gyro-kinetic equation in straight-field line coordinates. For the drift-type modes of interest, we use an eikonal representation for the perturbed ion distribution function; for the sake of completeness, we retain a finite radial mode number in the formulation of the problem. We identify the effects specific to the magnetic geometry. For a slow, drift-type mode, the plasma is in a quasineutrality condition. In turn, the quasineutrality condition requires a knowledge of the (fluctuating) electrostatic potential; the problem of closure is addressed Section 4 where the electron dynamics is presented.

One aim of this paper is to study the ion gyro-kinetic equation in fully 3d geometry. It is therefore convenient to write the confining magnetic field in straight-field-line coordinates as (Haeseleer *et al.* 1991)

$$\mathbf{B} = \nabla\alpha \times \nabla\psi \,, \tag{2}$$

where $\alpha \equiv \zeta - q\theta$ is the field line label and $2\pi\psi$ is the enclosed poloidal flux. Here θ and ζ are the poloidal and toroidal angle-like coordinates (with period 2π) respectively. Further, $s \equiv \Psi_{\rm T}/\Psi_{\rm T}^b$ is the normalised radial label, where $\Psi_{\rm T}$ is the enclosed toroidal flux within the magnetic surface and $\Psi_{\rm T}^b$ is $\Psi_{\rm T}$ evaluated at the plasma boundary. By construction, the radial label s runs from 0 (at the magnetic axis) to 1 (at the last closed magnetic surface). The effective radius of the magnetic surfaces is $r_{\rm eff} \equiv \bar{a}\sqrt{s}$, where $\bar{a}$ is the average minor radius of the last closed magnetic surface. We note that, in the coordinate system (s, θ, ζ), the Jacobian of the transformation, $\mathcal{J} \equiv [\nabla s \,.\, (\nabla\theta \times \nabla\zeta)]^{-1}$, has the dimensionality of a volume.

As is well known, the most unstable modes are characterised by $k_{||}/k_\perp \ll 1$, where $k_{||}$ and $k_\perp$ are the magnitude of the parallel and perpendicular components of the wavevector $\mathbf{k}$ respectively. The theory presented here is valid in the linear regime and the amplitude of the fluctuations are assumed to be small. For instance, a physical quantity F is written as $F = F_0 + \delta F$, where F_0 and δF are the equilibrium and perturbed parts of F, respectively, and $|\delta F/F_0| \ll 1$ is assumed. We exploit the smallness of $|\delta F/F_0|$ and $k_{||}/k_\perp$ by using the ballooning representation (Connor *et al.* 1978, 1979; Antonsen and Lane 1980)

$$\widetilde{F} \equiv \frac{\delta F}{F_0} \;= \widehat{F}\exp\left(i\frac{S}{\epsilon}\right), \tag{3}$$

where S is the eikonal and $\epsilon \ll 1$ is a smallness parameter (expansion parameter). The eikonal and the amplitude $\widehat{F}$ are assumed to vary on the equilibrium scale length so that the ordering $|\overline{R}\nabla\widehat{F}| \sim |\overline{R}\nabla S| = \mathcal{O}(1)$ is assumed. Formally, the amplitude $\widehat{F}$ must be expanded in ascending powers of ϵ. Following Antonsen and Lane (1980) we demand that the eikonal satisfies $\mathbf{B} \,.\, \nabla S = 0$ to all orders in ϵ. The spatial variation of $\widehat{F}$ represents the deviation from flute-like modes.

In stellarator geometry, one can use the extended toroidal angle ζ (instead of θ as in the tokamak case) as a label along the field line and the amplitude in equation (3) is written as $\widehat{F} = \widehat{F}(\zeta, t)$. To recover the standard form of the normal mode analysis, we make the transformation $\widehat{F}(\zeta, t) \mapsto \widehat{F}(\zeta)\exp(-i\omega t)$,

where ω is the normal mode frequency. The requirement $\mathbf{B} \cdot \nabla S = 0$ implies that $S = S(\alpha, q)$, where here q is used as a radial instead of s or ψ. It is natural to introduce the lowest-order perpendicular wavevector as (Antonsen and Lane 1980)

$$\begin{aligned} \mathbf{k}_\perp &\equiv \epsilon^{-1} \nabla S \\ &= \epsilon^{-1} \frac{\partial S}{\partial \alpha} \, (\nabla \alpha + \theta_k \nabla q) \\ &= n \frac{\partial S}{\partial \alpha} \, (\nabla \alpha + \theta_k \dot{q} \nabla s) \,, \end{aligned} \tag{4}$$

where $\theta_k \equiv (\partial S/\partial q)/(\partial S/\partial \alpha)$ and $n \equiv 1/\epsilon \gg 1$. A dot denotes a derivative with respect to the normalised radial label s. For simplicity, we consider an eikonal of the form $S = \alpha + \overline{S}$, and θ_k can now be seen as a free parameter (or 'radial mode number'). With this simplification, the lowest-order perpendicular wavevector reads

$$\mathbf{k}_\perp = n[\nabla \zeta - q \nabla \theta - \dot{q}(\theta - \theta_k) \nabla s] \,, \tag{5}$$

and n can be interpreted as the toroidal mode number. The left-hand side of equation (3) must satisfy the periodicity requirements in the poloidal and toroidal directions. The phase factor on the right-hand side of equation (3), however, is clearly not a periodic function of θ and ζ when the global shear is nonzero, $\dot{q} \neq 0$. Therefore one has to consider the amplitude $\widehat{F}$ to be defined on the covering space, $\zeta = [-\infty, +\infty]$. The problem of periodicity requirements in toroidal systems has been discussed by Antonsen and Lane (1980) and Connor *et al.* (1978). In this paper, we are concerned with the fastest linear growth rate and the *global* mode structure has not been (numerically) calculated. For *ideal* ballooning modes, one can use a ray tracing algorithm to determine the spectrum.

Ion Gyro-kinetic Equation

In this section we describe the assumptions used in our model. We write the collisionless ion gyro-kinetic equation in a form convenient for numerical work and identify the quantities which depend on the structure of **B**. Some intermediate steps in the derivation that were left out in a previous paper (Lewandowski 1998) are given and discussed.

We consider a low-β plasma with singly-charged ions and the magnetic perturbations are neglected. In such a plasma the (fluctuating) electric field is derivable from a potential, $\mathbf{E} = -\nabla \Phi$, where Φ is the fluctuating electrostatic potential. We also assume that collisional and trapping effects on the ion dynamics can be neglected. This neglect cannot always be justified, especially in the highly inhomogeneous magnetic field of a stellarator plasma.

For the sake of simplicity, we use the linear, collisionless gyro-kinetic equation for the ions. On the other hand, the electron population is assumed to be in the collisional regime (low T_e) and, again, particle trapping is neglected. Fluid equations (Braginskii 1965) are used to describe the electron dynamics. Therefore

the DTEM, and many other trapped particle modes, cannot be study with our model. Trapped particles and collisional effects can be treated accurately with the code developed by Kotschenreuther *et al.* (1988, 1992) for tokamak geometry using the $\hat{s} - \alpha$ model (Connor *et al.* 1978).

The method used in the present model is the following. The perturbed ion density is obtained by solving the ion gyro-kinetic equation while the perturbed electron density is calculated from fluid equations. These quantities depend on the electrostatic potential and we use the quasineutrality condition

$$n_{\rm i}(\Phi) = n_{\rm e}(\Phi)\,, \tag{6}$$

as a closure relation. The perturbed ion density is determined below and the perturbed electron density is given in Section 4.

Making use of the ballooning representation (3), the fluctuating electrostatic potential can be written in normalised form as

$$\widetilde{\Phi} \equiv \frac{e\Phi}{T_{\rm e0}} = \widehat{\Phi} \exp\left(i\frac{S}{\epsilon}\right), \tag{7}$$

where $T_{\rm e0}$ is the equilibrium electron temperature. We note that the equilibrium distribution for the ions must be independent of the gyro-angle and constant along the magnetic field line (Antonsen and Lane 1980; Frieman and Chen 1982; Taylor and Hastie 1968; Rutherford and Frieman 1968). These requirements are fulfilled for a Maxwellian distribution provided the equilibrium plasma density and ion temperature satisfy $\nabla_{||} n_0 = \nabla_{||} T_{\rm i0} = 0$, which is automatically satisfied since n_0 and $T_{\rm i0}$ are flux surface quantities. Since we are interested in small departures from thermodynamic equilibrium, it is a good approximation to set the parallel gradients of the equilibrium ion temperature and plasma density to zero. We assume that the equilibrium ion distribution function is indeed a Maxwellian

$$F_{\rm Mi} = \frac{n_0}{\pi^{\frac{3}{2}} {v_{\rm thi}}^3} \ \exp\left(-\frac{v^2}{{v_{\rm thi}}^2}\right), \tag{8}$$

where $v_{\rm thi} \equiv \sqrt{2T_{\rm i0}/m_{\rm i}}$ is the ion thermal velocity.

Following Xu and Rosenbluth (1991*a*), the amplitude of the perturbed ion distribution function can be written as

$$\widehat{f}_{\rm i} = -\frac{\widehat{\Phi}}{\tau}\ F_{\rm Mi} + \left(\widehat{h}_{\rm i} + \frac{\widehat{\Phi}}{\tau}\ J_0 F_{\rm Mi}\right) J_0\,, \tag{9}$$

where the nonadiabatic part $\widehat{h}_{\rm i}$ satisfies the linear, collisionless gyro-kinetic equation

$$\frac{\partial \widehat{h}_{\rm i}}{\partial t} = -v_{||}\nabla_{||}\left(\widehat{h}_{\rm i} + \frac{\widehat{\Phi}}{\tau}\ F_{\rm Mi} J_0\right) - i\ \omega_{\rm di}\ \widehat{h}_{\rm i} + i(\omega_{\star \rm i}^T - \omega_{\rm di})\frac{\widehat{\Phi}}{\tau}\ F_{\rm Mi} J_0\,. \tag{10}$$

In equations (9) and (10), $\tau \equiv T_{\rm i0}/T_{\rm e0}$, J_0 is the zeroth-order Bessel function (arising from the averaging over the fast gyro-motion) with argument $\xi_\perp \equiv k_\perp v_\perp/\omega_{\rm ci}$,

$k_\perp = \sqrt{\mathbf{k}_\perp \,.\, \mathbf{k}_\perp}$ is the magnitude of the lowest-order perpendicular wavevector and $\omega_{\rm ci} \equiv eB/m_{\rm i}c$ is the ion cyclotron frequency. Note that $\xi_\perp$ depends on the perpendicular velocity as well as the position along the field line through the dependence of B and $k_\perp$. The effect of the global magnetic shear manifests itself in the secular behaviour of $k_\perp$.

The first term on the right-hand side of equation (9) is the adiabatic part of the perturbed ion distribution function, while the last term represents the contribution from the polarisation. The polarisation term arises because the guiding centre density and the particle density do not coincide when the ion Larmor radius is finite. For instance, in an infinitely magnetised plasma, $B \mapsto \infty$, then $\xi_\perp \mapsto 0$ and $J_0 \mapsto 1$; in this case $\widehat{f_{\rm i}} \mapsto \widehat{h_{\rm i}}$, that is to say the guiding centre density and the particle density are equal, as they should be.

In equation (10)

$$\omega_{\star {\rm i}}^T \equiv \frac{cT_{\rm i}}{eBF_{\rm Mi}} \; (\widehat{\mathbf{e}}_{||} \times \mathbf{k}_\perp) \,.\, \nabla F_{\rm Mi} \tag{11}$$

is the velocity-dependent ion diamagnetic drift frequency, and

$$\omega_{\rm di} \equiv {\omega_{\rm ci}}^{-1} \left[\widehat{\mathbf{e}}_{||} \times \left({v_{||}}^2 \boldsymbol{\kappa} + \frac{{v_\perp}^2}{2} \; \frac{\nabla B}{B} + \frac{e}{m_{\rm i}} \; \nabla \Phi_0 \right) \right] \,.\, \mathbf{k}_\perp \,, \tag{12}$$

is the velocity-dependent ion curvature drift frequency, $\widehat{\mathbf{e}}_{||} \equiv \mathbf{B}/B$ is the unit vector along $\mathbf{B}$, $\boldsymbol{\kappa}$ is the magnetic curvature, Φ_0 is the equilibrium electrostatic potential and $\nabla_{||}$ is the parallel gradient operator keeping the field line label constant. For simplicity, we neglect the equilibrium electric field $\mathbf{E}_0 = -\nabla \Phi_0 = 0$. A nonvanishing $\mathbf{E}_0$ implies the presence of equilibrium plasma flows, which are neglected in the gyro-kinetic equation (10). Furthermore, in the presence of plasma flows, the ballooning representation (3) must also be modified (Artun and Tang 1992; Waelbroeck and Chen 1991; Cooper 1988).

The perturbed ion density is obtained by direct integration of equation (9). Introducing the amplitude of the normalised perturbed ion density $\widehat{n_{\rm i}} \equiv \widehat{\delta n_{\rm i}}/n_0$ we obtain

$$\widehat{n_{\rm i}} = -\frac{\widehat{\Phi}}{\tau} \; \int d^3 \; v \frac{F_{\rm Mi}}{n_0} \; + \frac{1}{n_0} \; \int d^3 v \; J_0 \; F_{\rm Mi} \; \widehat{g} + \frac{\widehat{\Phi}}{\tau} \; \int d^3 v \; {J_0}^2 \; \frac{F_{\rm Mi}}{n_0} \,, \tag{13}$$

where $\widehat{g} \equiv \widehat{h_{\rm i}}/F_{\rm Mi}$. The second integral on the right-hand side of equation (13) is computed numerically once $\widehat{g}$ is known (Section 4). After an appropriate change of variable, the last integral can be written as (Abramowitz and Stegun 1983)

$$\begin{aligned} \frac{1}{n_0} \; \int d^3 v \; {J_0}^2 \; F_{\rm Mi} &= \frac{1}{b_{\rm i}} \; \int_0^{+\infty} dy \; y \; {J_0}^2(y) \exp\left(- \frac{y^2}{2b_{\rm i}} \right) , \\ &= I_0(b_{\rm i}) \exp(-b_{\rm i}) \,, \end{aligned} \tag{14}$$

where I_0 is the modified Bessel function of zeroth order with argument $b_{\rm i} \equiv (k_\perp \rho_{\rm thi})^2/2$ and $\rho_{\rm thi}$ is the ion thermal gyro-radius. Substituting equation

(14) in (13), the quasineutrality condition (6) yields an equation for the perturbed electrostatic potential

$$\widehat{\Phi} = \frac{\tau}{G(b_\mathrm{i})} \left[\widehat{n_\mathrm{e}} - \frac{2}{\sqrt{\pi}} \int_0^\infty dx_\perp \int_{-\infty}^{+\infty} dx_{||} x_\perp J_0(\xi_\perp) \widehat{g} \exp(-{x_{||}}^2 - {x_\perp}^2) \right], \quad (15)$$

where $x_{||} \equiv v_{||}/v_\mathrm{thi}$, $x_\perp \equiv v_\perp/v_\mathrm{thi}$ and $\xi_\perp = \sqrt{2b_\mathrm{i}} x_\perp$. Here $\widehat{n_\mathrm{e}}$ represents the amplitude of the normalised electron density perturbation and is yet undetermined. We have also introduced $G(b_\mathrm{i}) \equiv I_0(b_\mathrm{i}) \exp(-b_\mathrm{i}) - 1$ which scales linearly with its argument in the long-wavelength limit.

Returning to the ion gyro-kinetic equation, one can show that

$$\omega_\mathrm{di} = 2\, \tau\, \omega_{\star\mathrm{e}}\, \epsilon_n \xi_d(\zeta) \left({x_{||}}^2 + \frac{{x_\perp}^2}{2} \right), \quad (16)$$

$$\omega_{\star\mathrm{i}}^\mathrm{T} = -\tau\, \omega_{\star\mathrm{e}}\, \xi_\star(\zeta) [1 + \eta_\mathrm{i} ({x_{||}}^2 + {x_\perp}^2 - \tfrac{3}{2})] \,. \quad (17)$$

Here $\omega_{\star\mathrm{e}} \equiv cT_{\mathrm{e}0} k_\theta / eB_0 L_n$ is the electron diamagnetic drift frequency; $k_\theta \equiv nq/\bar{a}$ is the characteristic magnitude of the perpendicular wavevector; $\eta_\mathrm{i} \equiv L_n/L_{\mathrm{T}\mathrm{i}}$; B_0 is the magnetic field strength at the magnetic axis; $\epsilon_n \equiv L_n/\bar{R}$ is the toroidicity parameter;

$$\xi_\star(\zeta) \equiv \frac{B_0}{B}\, \bar{a} \nabla s \,.\, (\widehat{\mathbf{e}}_{||} \times \widehat{\mathbf{e}}_\perp) \,, \quad (18)$$

where $\widehat{\mathbf{e}}_\perp \equiv \mathbf{k}_\perp / k_\theta$ is the normalised perpendicular wavevector; and finally

$$\xi_d(\zeta) \equiv \frac{B_0}{B}\, \widehat{\mathbf{e}}_\perp \,.\, \left(\widehat{\mathbf{e}}_{||} \times \frac{\bar{R} \nabla B}{B} \right). \quad (19)$$

All the terms on the right-hand sides of equations (18) and (19) are evaluated along the magnetic field line. After straightforward algebra, the normalised gyro-kinetic equation reads

$$\frac{\partial \widehat{g}}{\partial t''} = -\Omega_\mathrm{bi}\, \epsilon_n x_{||}\, \xi_{||}\, (\zeta) \frac{\partial}{\partial \zeta} \left(\widehat{g} + \frac{\widehat{\Phi}}{\tau}\, J_0 \right) - i\, \Omega_\mathrm{di}\, \widehat{g} + i\, (\Omega_{\star\mathrm{i}}^\mathrm{T} - \Omega_\mathrm{di}) \frac{\widehat{\Phi}}{\tau} \,, \quad (20)$$

where $\Omega_\mathrm{bi} \equiv v_\mathrm{thi}/\omega_{\star\mathrm{e}} L_n = \sqrt{2\tau/b}$, $\Omega_\mathrm{di} \equiv \omega_\mathrm{di}/\omega_{\star\mathrm{e}}$ and $\Omega_{\star\mathrm{i}}^\mathrm{T} = \omega_{\star\mathrm{i}}^\mathrm{T}/\omega_{\star\mathrm{e}}$. We have introduced the normalised time $t'' \equiv \omega_{\star\mathrm{e}} t$ and the parameter $b \equiv (k_\theta \rho_{s0})^2$, where ρ_{s0} is ρ_s evaluated at the magnetic axis. Here, $\xi_{||}(\zeta) \sim 1$ arises from the parallel gradient operator (keeping α constant)

$$\nabla_{||} = \frac{\xi_{||}(\zeta)}{\bar{R}}\, \frac{\partial}{\partial \zeta} \,. \quad (21)$$

The nondimensional quantities $\xi_{||}(\zeta)$, $\xi_d(\zeta)$ and $\xi_\star(\zeta)$ have been derived elsewhere (Lewandowski and Ellem 1999).

The remaining quantities that depend on the details of the magnetic field are b_i, which enters the quasineutrality condition, and $\xi_\perp$, which is the argument of the Bessel function in the gyro-kinetic equation. It can be shown that these quantities can be written as $\xi_\perp = \sqrt{2\tau b}\, x_\perp\, P(\zeta)$ and $b_\mathrm{i} = \tau b P^2(\zeta)$ where

$$P(\zeta) \equiv B_0 \frac{\sqrt{\widehat{\mathbf{e}}_\perp \,.\, \widehat{\mathbf{e}}_\perp}}{B}\,. \tag{22}$$

4. Electron Dynamics

The perturbed electron density, which is yet unspecified, is required in the quasineutrality condition (15). One possible model is to simply assume that the transport along the field line is large enough to short-circuit charge separation. In this case, the electron response is adiabatic so that $\widehat{n_\mathrm{e}} \simeq \widehat{\Phi}$. However, if the temperature of the electrons is not too large, then ion–electron collisions can prevent the electron density perturbation from reaching a Boltzmann distribution.

We can use a fluid model to obtain the perturbed electron density $\widehat{n_\mathrm{e}}$ provided the parallel wavelength of the mode is much larger than the electron mean free path. The electron mean free path, denoted λ_e, scales like ${T_\mathrm{e}}^2/n$, and it is therefore strongly dependent on the electron temperature.

With $k_{||}$ denoting the magnitude of the parallel wavevector, we assume that $k_{||}\lambda_\mathrm{e} \sim \epsilon$, where ϵ is a smallness parameter. The second requirement for a fluid theory to be applicable is that the characteristic perpendicular wavelength of the mode must be larger than the electron thermal gyro-radius. For our modes of interest, this condition is largely satisfied. For instance, for an isothermal discharge ($T_\mathrm{e} \simeq T_\mathrm{i}$), we have $k_\perp \rho_\mathrm{the} \sim (m_\mathrm{e}/m_\mathrm{i})^{\frac{1}{2}} k_\perp \rho_\mathrm{thi} \sim (m_\mathrm{e}/m_\mathrm{i})^{\frac{1}{2}} \ll 1$, assuming $k_\perp \rho_\mathrm{thi} \sim 1$. The most stringent condition is thus $k_{||}\lambda_\mathrm{e} = \mathcal{O}(\epsilon)$.

Another possible approach is to use the drift-kinetic equation for the electrons. However, the solution of the electron drift kinetic equation requires a careful treatment of regions of trapping and circulating electrons (Dominguez *et al.* 1992). For simplicity we neglect trapped electrons, even though the fraction of trapped electrons can be substantial in stellarator plasmas.

Our aim is to derive an equation which relates the perturbed electron density to the perturbation in the electrostatic potential. In general, the electron temperature fluctuations must be retained in the model (Lewandowski 1997*a*, 1997*b*, 1997*c*). The treatment of temperature fluctuation requires an additional equation, the energy equation. For simplicity, we also neglect temperature fluctuations. Hence our model equations are the electron continuity equation (Braginskii 1965)

$$\frac{\partial n_\mathrm{e}}{\partial t} + \nabla \,.\, (n_\mathrm{e} \mathbf{V}_\mathrm{e}) = 0\,, \tag{23}$$

and the electron momentum equation

$$e n_\mathrm{e} \left(\mathbf{E} + \frac{\mathbf{V}_\mathrm{e} \times \mathbf{B}}{c} \right) + \nabla p_\mathrm{e} = \mathbf{R}_\mathrm{ei}\,. \tag{24}$$

In equations (24) and (25), $\mathbf{V}_\mathrm{e}$ is the electron *fluid* velocity and $p_\mathrm{e} = n_\mathrm{e} T_\mathrm{e}$ is the electron pressure. In (24) we have neglected the electron inertia and the

electron stress tensor. The term on the right-hand side of the electron momentum equation is the friction force arising from electron–ion collisions which, for a plasma with singly-charged ions, is (Braginskii 1965)

$$\mathbf{R}_{\rm ei} = \eta_{||}\mathbf{J}_{||} + \eta_{\perp}\mathbf{J}_{\perp} - 0{\cdot}71\; n_{\rm e}\nabla_{||}T_{\rm e} - \frac{3\; n_{\rm e}}{2\;\omega_{\rm ce}\tau_{\rm e}}\;\widehat{\mathbf{e}}_{||}\times\nabla T_{\rm e}\,. \tag{25}$$

Here $\eta_{||}$ and $\eta_{\perp}$ are the parallel and perpendicular classical resistivities respectively; the parallel and perpendicular current densities are denoted $\mathbf{J}_{||}$ and $\mathbf{J}_{\perp}$ respectively; $\omega_{\rm ce} \equiv (eB)/(m_{\rm e}c)$ is the electron cyclotron frequency; and, finally, $\tau_{\rm e}$ is the electron basic collisional time. In the low-frequency regime, $\omega/\omega_{\rm ci} \sim \epsilon \ll 1$, we can solve equation (24) perturbatively for $\mathbf{V}_{\rm e\perp}$ yielding

$$\mathbf{V}_{\rm e\perp} = \mathbf{V}_E + \mathbf{V}_{de} + \mathbf{V}_c\,, \tag{26}$$

where

$$\mathbf{V}_E \equiv \frac{c}{B}\;\mathbf{E}\times\widehat{\mathbf{e}}_{||}, \quad \mathbf{V}_{de} \equiv \frac{c}{en_{\rm e}B}\;\nabla p_{\rm e}\times\widehat{\mathbf{e}}_{||}, \quad \mathbf{V}_c \equiv \frac{c}{en_{\rm e}B}\;\widehat{\mathbf{e}}_{||}\times\mathbf{R}_{\rm ei}\,, \tag{27}$$

are the lowest-order $\mathbf{E}\times\mathbf{B}$ drift velocity, the electron diamagnetic drift velocity and the ion-electron collision-driven drift velocity respectively. The last contribution in equation (26) is $(\omega_{\rm ce}\tau_{\rm e})^{-1}$ times smaller than $\mathbf{V}_E$ or $\mathbf{V}_{de}$. For a low-$T_{\rm e}$, high-density edge plasma, one gets $\omega_{\rm ce}\tau_{\rm e} \approx 10^5$. To a good approximation the perpendicular electron flux can be written as $\mathbf{\Gamma}_{\rm e\perp} \simeq n_{\rm e}(\mathbf{V}_E + \mathbf{V}_{de})$. Taking the scalar product of equation (24) with $\mathbf{B}$ and neglecting the electron temperature fluctuation yields

$$\eta_{||}J_{||} = p_{\rm e0}\nabla_{||}\widehat{h}\,, \tag{28}$$

where $\widehat{h} \equiv \widehat{n_{\rm e}} - \widehat{\Phi}$ is the nonadiabatic response of the electrons. We have neglected the equilibrium parallel current density when deriving equation (28); this is a low-β approximation and is well justified in small and medium size stellarator plasmas. If $J_{||0}$ is retained in the model, one can study the current-driven instability (Coppi and Mazzucato 1971).

Using equation (28), the divergence of the parallel electron flux is given by

$$\nabla\,.\,\mathbf{\Gamma}_{\rm e||} = \nabla\,.\,\mathbf{\Gamma}_{\rm i||} - \frac{1}{e}\;\nabla\,.\,\mathbf{J}_{||}\,. \tag{29}$$

We pay special attention to the geometrical details. In particular we note that, in the low-β approximation,

$$\begin{aligned}
\nabla\,.\,\mathbf{V}_E &= -\,2\,\frac{\nabla B}{B}\;.\,\mathbf{V}_E\,,\\
\nabla\,.\,(n_{\rm e}\mathbf{V}_{de}) &= -\,2\,n_{\rm e}\,\frac{\nabla B}{B}\;.\,\mathbf{V}_{de}, \quad \nabla\,.\,\widehat{\mathbf{e}}_{||} = -\widehat{\mathbf{e}}_{||}\,.\,\frac{\nabla B}{B}\,.
\end{aligned} \tag{30}$$

All these terms are curvature effects that vanish in slab geometry. The divergence of the perpendicular electron flux reads

$$\nabla \cdot \mathbf{\Gamma}_{\mathrm{e}\perp} = \mathbf{\Gamma}_E \cdot \left(\frac{\nabla n_{\mathrm{e}}}{n_{\mathrm{e}}} \; - \; 2\frac{\nabla B}{B} \right) - 2\mathbf{\Gamma}_{de} \cdot \frac{\nabla B}{B} \,, \tag{31}$$

where we have introduced $\mathbf{\Gamma}_E \equiv n_{\mathrm{e}}\mathbf{V}_E$ and $\mathbf{\Gamma}_{de} \equiv n_{\mathrm{e}}\mathbf{V}_{de}$. After straightforward algebra, using the ballooning representation, one gets

$$\nabla \cdot \mathbf{\Gamma}_{\mathrm{e}\perp} = i \; n_0 \; \omega_{\mathrm{e}\star} [S_\perp \widehat{n_{\mathrm{e}}} - (R_\perp + S_\perp)\widehat{\Phi}] \,, \tag{32}$$

where we have introduced two non-dimensional functions defined along the magnetic field line

$$R_\perp \equiv \bar{a}\nabla s \cdot \frac{(\widehat{\mathbf{e}}_{||} \times \widehat{\mathbf{e}}_\perp)}{B_\star}, \qquad S_\perp \equiv 2\mathbf{Q} \cdot \frac{(\widehat{\mathbf{e}}_{||} \times \widehat{\mathbf{e}}_\perp)}{B_\star} \,. \tag{33}$$

We have defined $\mathbf{Q} \equiv L_n \nabla B/B \sim \epsilon_n \equiv L_n/\overline{R}$ and we note that $\nabla \cdot \widehat{\mathbf{e}}_{||} = -Q_{||}/L_n$. Substituting equation (28) in (29) and using (32) in the electron continuity equation (23) yields

$$\begin{aligned} \frac{\partial \widehat{n_{\mathrm{e}}}}{\partial t''} = 2 \; \xi_c ({L_n}^2 \nabla_{||}{}^2 \widehat{h} - Q_{||} L_n \nabla_{||} \widehat{h}) - \frac{\nabla \cdot \mathbf{\Gamma}_{\mathrm{i}||}}{n_0 \omega_{\star \mathrm{e}}} \\ + i[(\xi_\star - 2 \; \epsilon_n \; \xi_d) \; \widehat{\Phi} + 2 \; \epsilon_n \; \xi_d \; \widehat{n_{\mathrm{e}}}] \,, \end{aligned} \tag{34}$$

where we have made use of the relations $R_\perp = \xi_\star$ and $S_\perp = -2\epsilon_n \xi_d$ and where we have introduced the 'collisional parameter' $\xi_c \equiv \omega_{\mathrm{ce}0}\tau_{\mathrm{e}}/k_\theta L_n$. Here $\omega_{\mathrm{ce}0}$ is the electron cyclotron frequency evaluated at the magnetic axis. For modes with $k_\theta \rho_s \sim 1$, it can be shown that the collisional parameter is much larger than unity. In slab geometry, one sets $Q_{||} = \xi_d = 0$ in equation (34).

The divergence of the parallel ion flux in equation (34) is determined directly from the perturbed ion distribution function (9). Letting $\widehat{H} \equiv J_0 \widehat{g} + \tau^{-1}\widehat{\Phi}({J_0}^2 - 1)$ we have $\widehat{f_{\mathrm{i}}} = F_{\mathrm{Mi}}\widehat{H}$. The divergence of the parallel ion flux is then

$$\nabla \cdot \mathbf{\Gamma}_{\mathrm{i}||} = \sqrt{2\tau/b} \; n_0 \; \omega_{\star \mathrm{e}} (L_n \nabla_{||} \widehat{\mathcal{L}} - Q_{||} \widehat{\mathcal{L}}) \,, \tag{35}$$

where

$$\widehat{\mathcal{L}} \equiv \frac{2}{\sqrt{\pi}} \; \int_0^\infty dx_\perp \int_{-\infty}^{+\infty} dx_{||} \; x_\perp \; x_{||} \; \exp(-{x_\perp}^2 - {x_{||}}^2) \widehat{H} \,. \tag{36}$$

Then the perturbed electron density is governed by the following time-dependent, linear equation:

$$\begin{aligned} \frac{\partial \widehat{n_{\mathrm{e}}}}{\partial t''} = 2 \; \xi_c ({L_n}^2 \nabla_{||}{}^2 \widehat{h} - Q_{||} L_n \nabla_{||} \widehat{h}) \\ + \sqrt{2\tau/b} (Q_{||} \widehat{\mathcal{L}} - L_n \nabla_{||} \widehat{\mathcal{L}}) + i(\xi_\star \widehat{\Phi} + 2 \; \epsilon_n \; \xi_d \; \widehat{h}) \,. \end{aligned} \tag{37}$$

The first term on the right-hand side of (37) describes the transport of current density along the magnetic field line, the second term represents the parallel ion *fluid* motion, and finally the third term is the transport of current density across the magnetic field.

5. Numerical Method

The numerical solution of equations (20) and (37) involves two kinds of difficulties. The first difficulty is associated with the secular terms, $\Omega_{\rm di}$, in the ion collisionless gyro-kinetic equation (20), and ξ_d, in the electron density equation (37). In the limit of large toroidal angle, it can be shown that these quantities scale linearly with ζ. Therefore, if the modes have a broad extent along the magnetic field line, the secular terms will be become important and the numerical integration then requires a small time step. It is worth noting that both $\Omega_{\rm di}$ and ξ_d, as well as $Q_{||}$, vanish in slab geometry.

Returning to the ion gyro-kinetic equation (20), we note that this equation is of the form

$$\frac{\partial \widehat{g}}{\partial t''} = -i\,\Omega_{\rm di}\,\widehat{g} + \ldots\,, \tag{38}$$

where the periodic terms and the contribution arising from the free streaming along $\mathbf{B}$ have been temporarily neglected. Clearly, at large values of the extended toroidal angle, $\Omega_{\rm di}$ is large and equation (38) can be numerically unstable, depending on the numerical method used. The equation for the perturbed electron density also contains a secular term similar to (38).

The second difficulty is associated with the different characteristic time scales of the ion and electron dynamics. In particular, the characteristic time scale of equation (37) is much smaller than the ion time scale. The electron characteristic time scale is small because the transport along the field line is large [terms mutiplied by the collisional parameter ξ_c in equation (37)].

The perturbed ion distribution is stored in a 3d array $\widehat{g}(\zeta, x_{||}, x_\perp)$ at each time step. The perturbed electron density $\widehat{n_{\rm e}}(\zeta)$ and the perturbed electrostatic potential $\widehat{\Phi}(\zeta)$ are stored in one-dimensional arrays at each time step. The infinite velocity domains of $x_{||}$ and $x_\perp$ are approximated by large finite domains. Specifically, a uniform grid for the (normalised) parallel velocity is setup as follows:

$$x_{||_p} = -x_{||\max} + (p-1)\Delta x_{||}\,, \tag{39}$$

where $\Delta x_{||} = 2x_{||\max}/(N_{||}-1)$, $x_{||\max}$ is the (positive-definite) maximum parallel velocity used in the integration, $N_{||}$ is the number of grid points and p is an integer running from 1 to $N_{||}$. Similarly, a uniform grid for the normalised perpendicular velocity is setup,

$$x_{\perp r} = (r-1)\Delta x_\perp\,, \tag{40}$$

where $\Delta x_\perp = x_{\perp\max}/(N_\perp - 1)$, $x_{\perp\max}$ is the maximum perpendicular velocity used in the integration and $N_\perp$ is the number of grid points. Here r is an integer which runs from 1 to $N_\perp$. The parameters $x_{||\max}, x_{\perp\max}, N_{||}$ and $N_\perp$ must be

varied to ensure the reliability of the results. Finally, a discrete grid along the toroidal angle is setup as follows:

$$\zeta_j = -\zeta_{\max} + (j - \tfrac{1}{2})\Delta\zeta\,, \tag{41}$$

where $\Delta\zeta = 2\,\zeta_{\max}/N_\zeta$ is the mesh size, $2\,\zeta_{\max}$ is the length of the domain of integration and the integer N_ζ is the number of grid points.

The perturbed distribution function for the ions is advanced in time using the Lax method (Press *et al.* 1983). The Lax method is appropriate when the parameter ϵ_n is not too large. It should be noted that the secular term ω_d is multiplied by the parameter ϵ_n. Introducing $\mathcal{D} \equiv \widehat{g} + \phi$ and $\phi \equiv J_0\widehat{\Phi}/\tau$, the nonadiabatic part of the perturbed ion distribution is updated in time according to (dropping the hats for clarity)

$$g_{jpr}^{(n+1)} = \tfrac{1}{2}\,\left[g_{j+1pr}^{(n)} + g_{j-1pr}^{(n)}\right] - C_{||jp}\frac{\Delta t}{2\Delta\zeta}\,\left[\mathcal{D}_{j+1pr}^{(n)} - \mathcal{D}_{j-1pr}^{(n)}\right]$$

$$- i\omega_{djpr}\,\Delta t\,\mathcal{D}_{jpr}^{(n)} + i\omega_{\star jpr}\,\Delta t\,\phi_{jr}^{(n)}\,, \tag{42}$$

where Δt is the time step of integration and n is an integer which labels the time step $(t_n = n\Delta t\,, n = 0, 1, 2, ...)$. Setting $\widehat{n}_e \mapsto N$ and dropping the hat notation, the electron continuity equation can be written as

$$\frac{\partial N}{\partial t} = D_{||}\frac{\partial^2 h}{\partial\zeta^2} - \beta_{||}\frac{\partial h}{\partial\zeta} - R_{||}\frac{\partial\mathcal{L}}{\partial\zeta}\;\; + W_{||}\mathcal{L} + 2i(\Phi + \epsilon_n\xi_d h)\,, \tag{43}$$

where

$$D_{||} \equiv 2\,\xi_c\,\xi_{||}^2\,\epsilon_n^2\,,$$

$$\beta_{||} \equiv \xi_c\,\xi_{||}\,\epsilon_n\left(2\,Q_{||} + \frac{\xi_{||}\epsilon_n}{\mathcal{J}}\;\frac{\partial\mathcal{J}}{\partial\zeta}\right),$$

$$R_{||} \equiv \sqrt{2\tau/b}\,\xi_{||}\,\epsilon_n, \qquad W_{||} \equiv \sqrt{2\tau/b}\,Q_{||}\,. \tag{44}$$

In equation (43) we have set $\xi_\star = 2$ (see next section).

The critical time step for the electrons is obtained by balancing the left-hand side of (43) with the diffusive term on the right-hand side ($\propto D_{||}$). If one uses an explicit method to advance the electron continuity equation, then the time step must be chosen so that

$$\Delta t \ll \Delta t_e = \frac{(\Delta\zeta)^2}{\xi_c\epsilon_n^2}\,. \tag{45}$$

We note the strongly unfavourable scaling with the mesh size $\Delta\zeta$. Furthermore, the collisional parameter ξ_c is quite large even for a moderate electron temperature ($\xi_c \sim 10^5$ for $T_e \sim 25$ eV). As we shall see below, the geometrical factors vary rapidly along ζ so that a small mesh size must be used. To bypass the stringent condition (45), it is advantageous to advance equation (43) in time using an

implicit method. The first and second terms and also the term with the secular contribution ξ_d are treated fully implicitly, while the remaining terms are treated with explicit finite differences. The resulting equation reads

$$a_j N_{j-1}^{(n+1)} + b_j N_j^{(n+1)} + c_j N_{j-1}^{(n+1)} = S_j^{(n)}\,, \tag{46}$$

where

$$\begin{aligned} a_j &= \frac{\Delta t}{\Delta\zeta}\,\left(\frac{\alpha_{||j}}{\Delta\zeta} + \frac{\beta_{||j}}{2}\right), \\ b_j &= -\left[1 + 2\,\frac{\alpha_{||j}\Delta t}{(\Delta\zeta)^2}\right], \\ c_j &= \frac{\Delta t}{\Delta\zeta}\left(\frac{\alpha_{||j}}{\Delta\zeta} - \frac{\beta_{||j}}{2}\right), \end{aligned} \tag{47}$$

and the 'source term' on the right-hand side of equation (46) is

$$\begin{aligned} S_j^{(n)} = {} & \frac{\alpha_{||j}\Delta t}{(\Delta\zeta)^2}\,[\Phi_{j+1}^{(n)} - 2\Phi_j^{(n)} + \Phi_{j-1}^{(n)}] - \frac{\beta_{||j}\Delta t}{2\Delta\zeta}[\Phi_{j+1}^{(n)} - \Phi_{j-1}^{(n)}] \\ & + 2\,i\Delta t(\epsilon_n - 1)\Phi_j^{(n)} + \frac{R_{||j}\Delta t}{2\Delta\zeta}\,[\mathcal{L}_{j+1}^{(n)} - \mathcal{L}_{j-1}^{(n)}] - N_j^{(n)}\,. \end{aligned} \tag{48}$$

The system of N_ζ equations (46) can be written as a tridiagonal matrix, which is solved using the LU decomposition method (Press *et al.* 1983). Note that the solution of (46) does not require pivoting, a feature which considerably improves the vectorisation of the numerical code. For all the runs presented in this paper, a vectorisation of $\geq 92\%$ was achieved.

6. Numerical Calculations

In this section, the model equations described in the previous section are solved numerically for the toroidal heliac H1-NF (Hamberger *et al.* 1990). The dependences of the linear growth rate and the real part of the mode frequency on the toroidal mode number and the η_{i} parameter are presented. Most of the calculations are performed for only one field line. However, we also present some results for a set of different field lines.

The 3d equilibrium state is computed using the VMEC equilibrium (Hirshman and Lee 1986; Hirshman and Betancourt 1991), with zero net toroidal current within each flux tube. The plasma pressure profile is of the form

$$p(s) = p(0)\,(1-s)^2\,. \tag{49}$$

The full equilibrium is computed for a set of 100 magnetic surfaces and for a volume-averaged $\overline{\beta}$ of $0{\cdot}36\%$. A poloidal cross section of the H1-NF plasma is shown in Fig. 1 in Lewandowski (1997*c*). A mapping code is used to specify the equilibrium in straight-field-line coordinates. The magnetic surfaces are specified in a series of Fourier harmonics. For instance, the position vector $\mathbf{r}$ is written in cylindrical coordinates as

$$\mathbf{r} = R\cos\phi\,\widehat{\mathbf{x}} + R\sin\phi\,\widehat{\mathbf{y}} + Z\,\widehat{\mathbf{z}}\,, \tag{50}$$

where

$$R = \sum_{m=0}^{M}\sum_{n=-N}^{n=+N} R_{mn}\ \cos(\mu_{mn})\,,$$

$$Z = \sum_{m=0}^{M}\sum_{n=-N}^{n=+N} Z_{mn}\ \sin(\mu_{mn})\,,$$

$$\phi = \zeta - \frac{2\pi}{N_p}\ \sum_{m=0}^{M}\sum_{n=-N}^{n=+N} \widetilde{\phi}_{mn}\sin(\mu_{mn})\,. \tag{51}$$

Here $\mu_{mn} \equiv m\theta + N_p n\zeta$ and $N_p = 3$ is the number of field periods of H1-NF. In equation (51), the input parameters are chosen as $N = 27$ and $M = 13$. Using equations (50) and (51) we can determine the covariant and contravariant basis vectors and any combinations of these quantities required in the calculations of equilibrium quantities such as $B(\zeta)$, $\xi_d(\zeta)$, $k_\perp(\zeta)$ and $\xi_{||}(\zeta)$.

We now calculate the explicit form of the geometrical quantities $\xi_d(\zeta)$, $k_\perp(\zeta)$ and $\xi_{||}(\zeta)$.

Following the same notation as earlier, we write the confining magnetic field in straight-field-line coordinates (SFLC) as $\mathbf{B} = \nabla\alpha \times \nabla\psi(s)$; here α is the field line label, $2\pi\psi$ is the enclosed poloidal flux and s is the (normalised) radial coordinate (defined earlier). Letting $\overline{\eta} \equiv \theta B_\theta(s) + \zeta B_\zeta(s)$, one can write the magnetic field in an alternative form

$$\mathbf{B} = \nabla\overline{\eta} + B_s^\star \nabla s\,, \tag{52}$$

where $B_s^\star \equiv B_s - \theta\dot{B}_\theta - \zeta\dot{B}_\zeta$ and, as before, a dot denotes a derivative with respect to s. Then the parallel gradient operator, keeping the radial label and the field line label constants, can be written as

$$\nabla_{||} \equiv \frac{\mathbf{B}\,.\,\nabla}{B}\ \Bigg|_{s,\alpha} = \frac{\mathbf{B}\,.\,\nabla\overline{\eta}}{B}|_{s,\alpha}\frac{\partial}{\partial\overline{\eta}} = B|_{s,\alpha}\frac{\partial}{\partial\overline{\eta}} = \frac{\xi_{||}}{\overline{R}}\ \frac{\partial}{\partial\zeta}\,, \tag{53}$$

where $\xi_{||}(\zeta) \equiv \overline{R}q\dot{\psi}/\mathcal{J}B$ is a non-dimensional function, defined along the extended toroidal angle, of the order of unity (in this expression B is evaluated at $\alpha = \alpha_0 = \text{const.}$).

The quantity related to the diamagnetic drift frequency $\xi_\star$ can be calculated as follows:

$$\xi_\star = -\frac{B_0\bar{a}^2}{Bq(s)}\ \nabla s\,.\left(\nabla\alpha \times \frac{\mathbf{B}}{B}\right) = \frac{B_0\bar{a}^2}{q(s)\dot{\psi}}\,, \tag{54}$$

where we have made use of the relation

$$B^2 = \dot{\psi}^2[\nabla\alpha\,.\,\nabla\alpha\ \nabla s\,.\,\nabla s - (\nabla s\,.\,\nabla\alpha)^2]\,. \tag{55}$$

Now we make use of the definition of the safety factor $q(s) \equiv \dot{\Psi}_{\rm T}/\dot{\Psi}_{\rm P}$, where $\Psi_{\rm T}$ and $\Psi_{\rm P}$ are the toroidal and poloidal fluxes enclosed within s respectively. By definition $\psi = \Psi_{\rm P}/2\pi$ while, by construction, $\Psi_{\rm T} = B_0 \pi \bar{a}^2 s$, from which we get $\dot{\psi} = \bar{a}^2 B_0/2q$. It follows that $\xi_\star = 2$.

We now calculate the normalised quantity $\xi_d(\zeta)$, related to the curvature drift frequency. After straightforward algebra, one can show that

$$\xi_d = \frac{\bar{a}\bar{R}B_0}{2q(s)B}\left[\left(\frac{\dot{F}}{F} - \frac{1}{\mathcal{J}}\,\frac{\partial \mathcal{J}}{\partial s}\right)\nabla\alpha\,.\,(\widehat{\mathbf{e}}_{||}\times\nabla s) - \frac{1}{\mathcal{J}}\,\frac{\partial \mathcal{J}}{\partial \theta}\,\nabla\alpha\,.\,(\widehat{\mathbf{e}}_{||}\times\nabla\theta)\right.$$
$$\left. - \frac{1}{\mathcal{J}}\,\frac{\partial \mathcal{J}}{\partial \zeta}\,\nabla\alpha\,.\,(\widehat{\mathbf{e}}_{||}\times\nabla\zeta)\right], \tag{56}$$

where, in Boozer (1980, 1981, 1982) coordinates, $F(s) \equiv \mathcal{J}B^2$ is a flux surface quantity. The final form for ξ_d (the form actually used in the code) reads

$$\xi_d(\zeta) = \frac{\bar{a}\bar{R}B_0}{2q\dot{\psi}}\left[\frac{1}{\mathcal{J}}\,\frac{\partial \mathcal{J}}{\partial s} - \frac{\dot{F}}{F}\right.$$
$$+ \frac{\dot{\psi}^2}{F}\,\frac{\partial \mathcal{J}}{\partial \theta}\,(\nabla\alpha\,.\,\nabla\alpha\,\nabla s\,.\,\nabla\theta - \nabla\theta\,.\,\nabla\alpha\,\nabla s\,.\,\nabla\alpha)$$
$$\left. + \frac{\dot{\psi}^2}{F}\,\frac{\partial \mathcal{J}}{\partial \zeta}\,(\nabla\alpha\,.\,\nabla\alpha\,\nabla s\,.\,\nabla\zeta - \nabla\zeta\,.\,\nabla\alpha\,\nabla s\,.\,\nabla\alpha)\right]. \tag{57}$$

The terms involving $\nabla\alpha = \nabla\zeta - q\nabla\theta - \dot{q}\theta\nabla s$ are responsible for the secular behaviour of ξ_d.

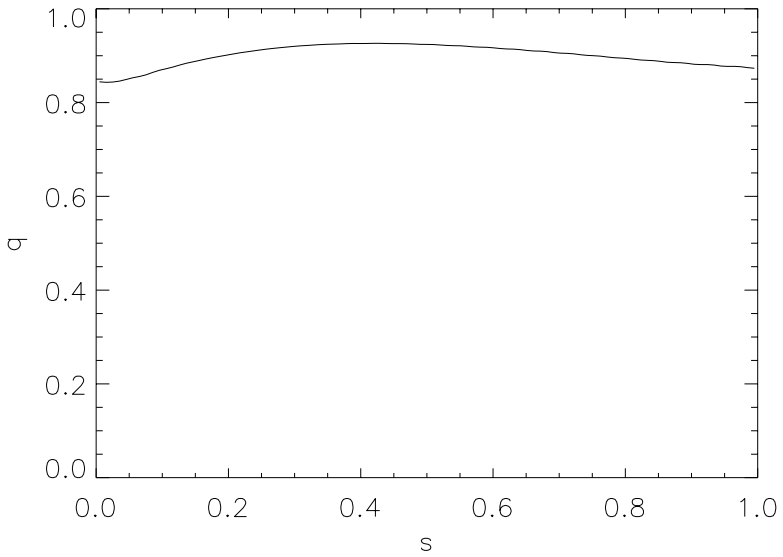

Fig. 1. Safety factor as a function of the normalised radial s for the standard configuration of the toroidal heliac H1-NF.

All the calculations are performed on the magnetic surface $s_0 = 0{\cdot}97$, which is shown in Fig. 1 in Lewandowski (1997*c*). A poloidal cross section of the magnetic surfaces at the plane $\phi = 0$ is also shown in Fig. 2 of that paper.

Except for Fig. 6*b*, all the calculations were carried out for the field line $\theta_0 = \zeta_0 = 0 \mapsto \alpha_0 = 0$. The point $(\theta_0 = 0, \zeta_0 = 0)$ is a symmetry point and each scalar physical quantity F must satisfy $F(-\zeta) = F(+\zeta)$.

The safety factor profile as a function of the normalised radial label s is shown in Fig. 1. The global shear is slightly negative for the magnetic surface used in our calculations ($s_0 = 0{\cdot}97$). The choice $s_0 = 0{\cdot}97$ corresponds to an effective local minor radius $\rho_0 = \sqrt{s_0}\bar{a} \simeq 0{\cdot}98\bar{a}$, that is the outboard side of the plasma where the destabilising influence of the normal curvature is the strongest. The choice $s_0 = 1{\cdot}0$ is difficult to implement since second-order derivatives in the radial label are nonlocal.

The linear growth rate, normalised to the electron diamagnetic drift frequency $\omega_{\star e}$, is computed as follows:

$$\gamma(t'') = \frac{1}{|\langle\widehat{\Phi}\rangle_\zeta|} \frac{\partial|\langle\widehat{\Phi}\rangle_\zeta|}{\partial t''}, \tag{58}$$

where $|G| \equiv (GG^\star)^{\frac{1}{2}}$ denotes the norm of G and $\langle\widehat{\Phi}\rangle_\zeta$ denotes an average along the magnetic field line

$$\langle\widehat{\Phi}\rangle_\zeta \equiv \frac{1}{2\zeta_{\rm m}} \int_{\zeta_0-\zeta_{\rm m}}^{\zeta_0+\zeta_{\rm m}} \widehat{\Phi}(\zeta')d\zeta'. \tag{59}$$

Here ζ_0 represents a toroidal angle of reference. Unlike the axi-symmetric tokamak configuration, the poloidal angle, θ_0, *and* the toroidal angle, ζ_0, must be given to specify the point of reference (on a given magnetic surface with radial position s_0). The real part of the mode frequency, normalised to $\omega_{\star e}$, is denoted $\omega_{\rm r}$. It is computed as follows:

$$\omega_{\rm r}(t'') = \Re\left(\frac{i}{\langle\widehat{\Phi}\rangle_\zeta} \frac{\partial\langle\widehat{\Phi}\rangle_\zeta}{\partial t''}\right), \tag{60}$$

where $\Re(\eta)$ denotes the real part of η. The derivations of equations (58) and (60) are given in the Appendix. The parameter $\zeta_{\rm m}$ must be chosen sufficiently large so that the growth rate (58) and the real part of the mode frequency (60) become independent of $\zeta_{\rm m}$ itself. The physically meaningful growth rate and real frequency are obtained for large t'', when $\partial\gamma/\partial t'' \simeq 0$ and $\partial\omega_{\rm r}/\partial t'' \simeq 0$.

For our calculations, we have chosen the following parameters: $x_{||\max} = v_{||\max}/v_{\rm thi} = 8$, $x_{\perp\max} = v_{\perp\max}/v_{\rm thi} = 4$, $N_{||} = 140$, $N_\perp = 70$, a mesh size $\Delta\zeta = \pi/100$ and a time step $\Delta t'' = 5 \times 10^{-3}$. These parameters have been varied to test their sensitivities. As it turns out, the growth rate at the end of the calculations is independent of $N_{||}$ and $N_\perp$ when $N_{||} \geq 40$ and $N_\perp \geq 20$. For simplicity, we used $\theta_k = 0$ in all our calculations. Strictly speaking, the parameter θ_k must be varied until the fastest linear growth rate is found; however, our choice $\theta_k = 0$ is motivated following a recent numerical analysis by Lewandowski

and Ellem (1999) which shows that $\partial\gamma/\partial\theta_k < 0$. At the beginning of the calculations, the perturbed ion distribution is assumed to be a small Maxwellian located around ζ_0 and the electron response is assumed to be adiabatic, $\widehat{n_e} = \widehat{\Phi}$. Then, the electrostatic potential is computed using equation (15) followed by the perturbed ion distribution function (20) and the perturbed electron density (37). The 'new' electrostatic potential can be computed from equation (15) and the process is repeated until convergence is obtained.

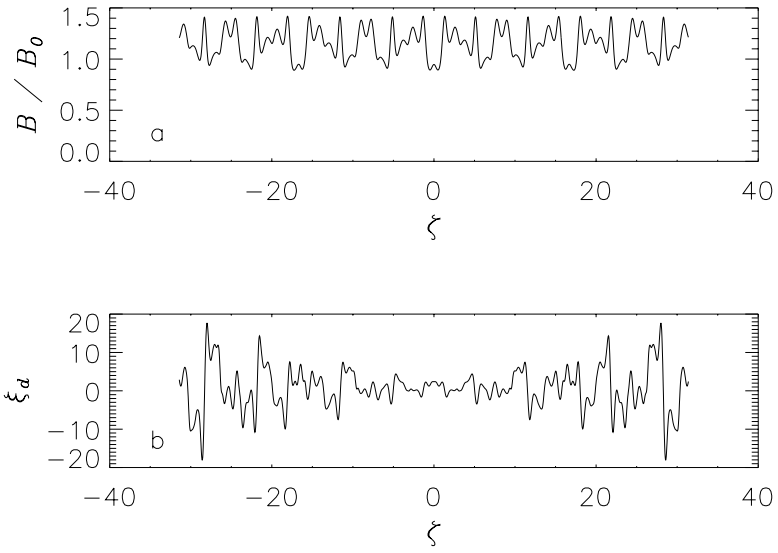

Fig. 2. Magnetic field strength and the normalised curvature drift frequency as a function of the extended toroidal angle. The field line of reference is $\theta_0 = \zeta_0 = 0$.

The magnetic field strength, normalised to the magnetic field strength at the magnetic axis, as a function of the extended toroidal angle is shown in Fig. 2*a*. The field line of reference is labeled $\theta_0 = \zeta_0 = 0$, which corresponds to $\zeta = 0$ in Fig. 2*a* [and $X = 6{\cdot}5$ cm, $Y = 0$ in Fig. 2 in Lewandowski (1997*c*]. The point $\theta_0 = \zeta_0 = 0$ is a symmetry point so that $B(+\zeta) = B(-\zeta)$. All scalar equilibrium quantities as well as the mode amplitude should be symmetric in ζ. We have chosen the point of reference $\theta_0 = \zeta_0 = 0$ because the destabilising influence of the normal curvature is the strongest at that point (see also the discussion at the end of this section). Fig. 2*b* shows the curvature drift term ξ_d, defined by equation (19), for the same field line as in Fig. 2*a*. The secular behaviour becomes important for $|\zeta| \geq 10$.

The time evolution of the growth rate and the real part of the mode frequency is shown in Fig. 3. The parameters are $\tau = 3$, $T_e = 15$ eV, $n_0 = 5 \times 10^{12}$ cm^{-3}, $L_n = 10$ cm, $k_\theta \rho_{s0} = 1{\cdot}0$ and $\eta_i = 2{\cdot}3$. These parameters are representative of H1-NF experimental conditions. The large electron transport along the field line ($\propto \xi_c \gg 1$) is responsible for the rapid variation of γ and ω_r for $t'' \leq 0{\cdot}01$. An equilibrium state is reached for $t'' \geq 0{\cdot}05$. The final value for the (normalised) growth rate and frequency are, respectively, $\gamma = 0{\cdot}155$ and $\omega_r = -0{\cdot}78$.

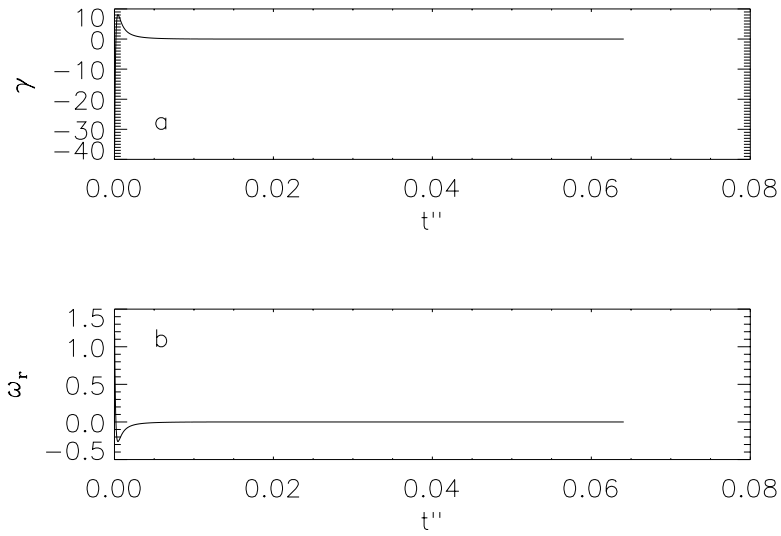

Fig. 3. Normalised growth rate and the real frequency as a function of the normalised time $t'' = \omega_{\star e} t$.

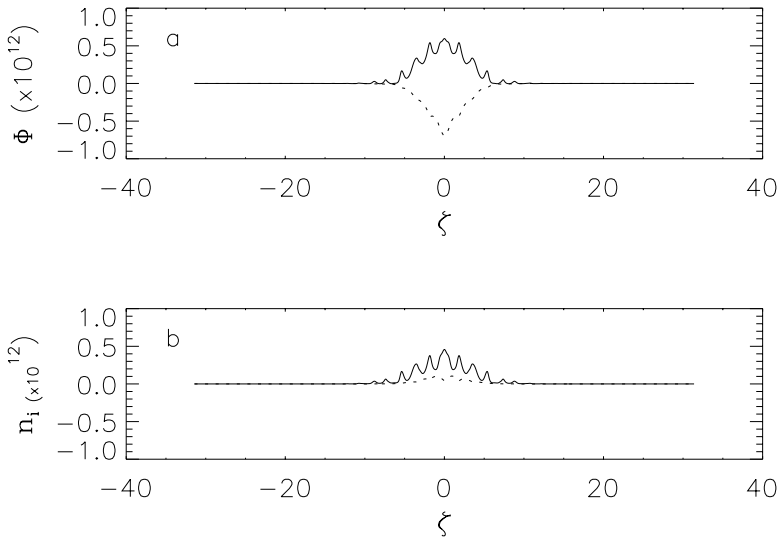

Fig. 4. Real (solid curve) and imaginary (dotted curve) parts of the eigenfunctions of (*a*) the electrostatic potential and (*b*) the ion density at the end of the calculations.

The eigenfunction of the electrostatic potential at the end of the calculations is shown in Fig. 4*a*. The mode has a ballooning character. The real part of $\widehat{\Phi}$ displays a rapid, coil-induced variation along ζ, superimposed to a slow, curvature-driven variation. The eigenfunction of the perturbed ion density at the end of the calculations is shown in Fig. 4*b*. The imaginary part of $\widehat{n_{\mathrm{i}}}$ is not in phase with the imaginary part of $\widehat{\Phi}$.

We now study the dependence of γ and ω_{r} on the toroidal mode number. Fig. 5 shows the real and imaginary parts of the mode frequency as a function of $k_\theta \rho_s$, for the field line of reference $\theta_0 = \zeta_0 = 0$. Other parameters are the same as in Fig. 2. The growth rate (Fig. 5*a*) peaks around $k_\theta \rho_s \simeq 0{\cdot}6$. For the parameters used in the calculations, the electron population is deeply in the collisional regime. The mode rotates in the ion direction, and ω_{r} becomes more negative as the toroidal mode number increases. However, for $k_\theta \rho_s \geq 0{\cdot}8$, the dependence of ω_{r} on the toroidal mode number is weak.

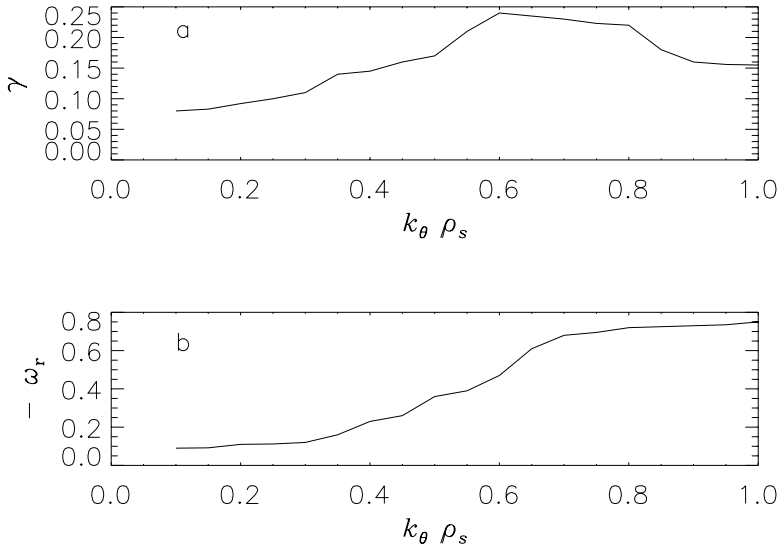

Fig. 5. Normalised growth rate and the real frequency as a function of $k_\theta \rho_s$ for the field of reference $\theta_0 = \zeta_0 = 0$.

We have also investigated the influence of the ion temperature gradient on the linear growth rate, while the density scale length is fixed. The dependence of γ as a function of the parameter η_{i} is shown in Fig. 6*a*. Other parameters are the same as in Fig. 2. At a small value of η_{i} the mode is stable, while for large ion temperature gradient (large η_{i}), the mode is unstable. The threshold is $\eta_{\mathrm{ic}} \simeq 1{\cdot}1$. It is interesting to note that a threshold η_{ic} of the order of unity is also typical of tokamak plasmas.

Finally, we have studied a set of different field lines, each of them having the same toroidal angle of reference $\zeta_0 = 0$. The poloidal angle of reference θ_0 has been increased from 0 to 2π. In real space, this corresponds to moving from the outboard side of the plasma ($\theta_0 = 0$) to the inboard side of the plasma ($\theta_0 = \pi$) and back again to the outboard side (see Fig. 2 in Lewandowski 1997*c*).

The linear growth rate as a function of θ_0 is shown in Fig. 6*b*. Interestingly, the maximum growth rate is at $\theta \simeq 2.7$, which corresponds to a point in the *inboard side* of the plasma where the normal curvature is *stabilising*. This result is surprising since one would expect the maximum growth rate to be found where the destabilising influence of the normal curvature is the strongest, that is at $\theta_0 = 0$. However, the curvature drive ξ_{d} depends on a combination of the normal curvature, the geodesic curvature, the integrated residual

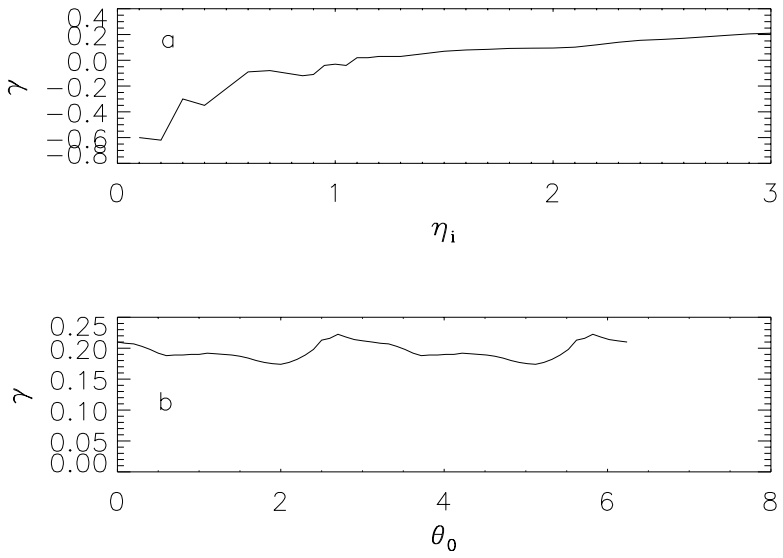

Fig. 6. (a) Normalised growth rate as a function of the ion temperature gradient parameter $\eta_{\rm i}$ for the same field line as in Fig. 4 and (b) for different field lines starting in poloidal cross section $\phi = 0$.

shear and the global shear. To show this we note that, in the low-β approximation, the magnetic curvature can be written as $\boldsymbol{\kappa} \equiv (\widehat{\mathbf{e}}_{||} \,.\, \nabla)\widehat{\mathbf{e}}_{||} \simeq \nabla_\perp B/B$. Since $\boldsymbol{\kappa} \,.\, \mathbf{B}$ identically vanishes, one can write (Haeseleer *et al.* 1991)

$$\boldsymbol{\kappa} = \kappa_{\rm N}\widehat{\mathbf{n}} + \kappa_{\rm G}\widehat{\mathbf{b}}\,, \tag{61}$$

where $\widehat{\mathbf{n}} \equiv \nabla\psi/\sqrt{g^{\psi\psi}}$ is the unit normal vector ($g^{\psi\psi} \equiv \nabla\psi \,.\, \nabla\psi$ is a metric element), $\widehat{\mathbf{b}} \equiv \widehat{\mathbf{e}}_{||} \times \widehat{\mathbf{n}}$ is the unit binormal vector, $\kappa_{\rm N} \equiv \boldsymbol{\kappa} \,.\, \widehat{\mathbf{n}}$ is the normal component of the magnetic curvature and $\kappa_{\rm G} \equiv \boldsymbol{\kappa} \,.\, \widehat{\mathbf{b}}$ is the geodesic component of the magnetic curvature. The curvature drive, defined by equation (19), can now be written as

$$\xi_d = \overline{R}\frac{B_0}{B}\ \widehat{\mathbf{e}}_\perp \,.\, \widehat{\mathbf{b}}(\kappa_{\rm N} - \mathcal{L}\kappa_{\rm G})\,, \tag{62}$$

where $\mathcal{L} \equiv (\widehat{\mathbf{n}} \,.\, \widehat{\mathbf{e}}_\perp)/(\widehat{\mathbf{b}} \,.\, \widehat{\mathbf{e}}_\perp)$. After straightforward algebra, one gets the following:

$$\begin{aligned} \widehat{\mathbf{e}}_\perp &= \frac{\overline{a}}{q}\ \left(\nabla\alpha + \theta_k\frac{dq}{d\psi}\ \nabla\psi\right), \\ \widehat{\mathbf{b}} &= \frac{1}{B\sqrt{g^{\psi\psi}}}\ (g^{\alpha\psi}\nabla\psi - g^{\psi\psi}\nabla\alpha)\,, \end{aligned} \tag{63}$$

where $g^{\alpha\psi} = \nabla\alpha \,.\, \nabla\psi$ is a metric element. Using the above equations, it follows that

$$\mathcal{L} = B\frac{g^{\alpha\psi} + \theta_k dq/d\psi \;\; g^{\psi\psi}}{(g^{\alpha\psi})^2 - g^{\alpha\alpha}g^{\psi\psi}} \,. \tag{64}$$

Writing the confining magnetic field in SFLC, $\mathbf{B} = \nabla\alpha \times \nabla\psi$, one can show that $B^2 = g^{\alpha\alpha}g^{\psi\psi} - (g^{\alpha\psi})^2$. After some manipulation, we obtain

$$\xi_d = -\frac{2A}{\sqrt{g^{ss}}}\left\{\kappa_{\rm N} - \frac{\nabla\psi\,.\,\nabla\psi}{B}\left[\mathcal{R} + (\theta - \theta_k)\frac{dq}{d\psi}\right]\kappa_{\rm G}\right\}, \tag{65}$$

where $A \equiv \overline{R}/\bar{a}$ is the aspect ratio and we have introduced the integrated residual shear

$$\mathcal{R} \equiv \frac{q\nabla\theta\,.\,\nabla\psi - \nabla\psi\,.\,\nabla\zeta}{\nabla\psi\,.\,\nabla\psi} \,. \tag{66}$$

Clearly, from equation (65), it is not sufficient to consider the point where the normal curvature is the most destabilising to determine the poloidal angle at which the growth rate is the largest. If the poloidal angle of reference θ_0 is varied, equation (65) shows that the combination of the geodesic curvature, the integrated residual shear and global shear modifies the drive arising from the normal curvature $\kappa_{\rm N}$. We note that for magnetic surfaces which strongly depart from perfect circularity (see Fig. 2 in Lewandowski 1997*c*), the factors g^{ss} and $\nabla\psi\,.\,\nabla\psi$ vary rapidly as one moves poloidally. In a tokamak with circular magnetic surfaces, the spatial variations of g^{ss} and $\nabla\psi\,.\,\nabla\psi$ are small. Furthermore, the integrated residual shear can be shown (Lewandowski and Persson 1995, 1996) to be much smaller than the remaining terms in equation (65). In the local approximation (θ and $\kappa_{\rm G}$ small), one gets $\xi_d \sim -2A\kappa_{\rm N}/\sqrt{g^{ss}}$. In this case, it is a good approximation to consider the sign of $\kappa_{\rm N}$ alone. In the strong global shear case ($dq/d\psi$ large), one has to retain the coupling between $dq/d\psi$ and the geodesic curvature.

7. Conclusion

We have studied the drift wave dynamics (in the linear approximation) in a toroidal heliac using a novel fluid/gyro-kinetic hybrid code. The calculations can be repeated for plasmas of arbitrary shape (provided their magnetic surfaces are nested).

The fluid/gyro-kinetic hybrid model is valid for $\tau \equiv T_{\rm i}/T_{\rm e} \geq 1$. Recent experiments in H1-NF (Shats *et al.* 1998) show that $2 \leq \tau \leq 10$, so that our model can be applicable. However, the observed plasma magnetisation is small and the fluctuating level is large, suggesting that a fully nonlinear model should be developed to interpret the experimental measurements.

A limitation of our model is the neglect of trapped particles (ions and electrons). As we can see in Fig. 2*a*, the magnetic field strength varies rapidly along the field line, and we can expect the particle trapping to be important. For H1-NF experimental parameters, a large fraction of H1-NF plasma might be sensitive to the dissipative trapped-electron mode (DTEM). However, since $T_{\rm i} \gg T_{\rm e}$, the study

of the DTEM* must be coupled to the full ion dynamics (including gyro-viscous effects). This is left for future work.

Most of the calculations presented in this paper were done for a vanishing radial mode number (which corresponds to $\theta_k = 0$). A previous numerical study (Lewandowski 1998) has shown that $\theta_k = 0$ yields the fastest growth rate, although this conclusion is specific to a configuration with small global magnetic shear.

One of the main results reported in the present paper is the calculation of the threshold of the ion temperature gradient parameter $\eta_{\rm ic}$. For the field line passing through the reference point $(s_0 = 0{\cdot}97, \theta_0 = 0, \zeta_0 = 0)$, we have found that $\eta_{\rm ic} \simeq 1{\cdot}1$. In general, the threshold will be different on different field lines, that is $\eta_{\rm ic} = \eta_{\rm ic}(s_0, \theta_0, \zeta_0)$. For a low-shear configuration such as H1-NF (Fig. 1), the threshold depends weakly on the radial label so that

$$\frac{\partial \eta_{\rm ic}}{\partial s_0} \ll \frac{\partial \eta_{\rm ic}}{\partial \theta_0} \quad \text{and} \quad \frac{\partial \eta_{\rm ic}}{\partial s_0} \ll \frac{\partial \eta_{\rm ic}}{\partial \zeta_0} \,. \tag{67}$$

When the ion temperature gradient parameter $\eta_{\rm i} = \eta_{\rm i}(s_0)$ (flux surface quantity) is close to its threshold value for that particular magnetic surface, the magnetic surface s_0 can be divided into two regions: $\eta_{\rm i} > \eta_{\rm ic}$ (region U) and $\eta_{\rm i} \leq \eta_{\rm ic}$ (region S). As a consequence, the mode is growing exponentially in region U but it is stable in region S: as a result we might expect *convection* processes to take place between these two regions (even in the *linear* regime). How these convection processes will affect the cross-field (anomalous) transport is beyond the scope of the present paper, and it is left for future work.

We have also studied the drift wave spectrum for one field line. For the field line $\theta_0 = \zeta_0 = 0$, we have shown that the largest linear growth rate occurs at $k_\theta \rho_s \simeq 0{\cdot}6$. This result can be understood by inspection of the electron equation (37). The parallel ion motion in (37) is given by the second term on the right-hand side. This term varies as $b^{-1/2} = 1/k_\theta \rho_s$ and we can expect a qualitative change around $k_\theta \rho_s \sim 1$.

A limitation of our model is the neglect of trapped particles (ions and electrons). In a stellarator plasma, the magnetic field strength varies rapidly along the field line (see e.g. Fig. 4 in Lewandowski 1997*b*), and we can expect the particle trapping to be important. If the electrons are cold, such as in the H1-NF experiments (Shats *et al.* 1998), then the (magnetic) trapping can be safely neglected. For the ion population, however, the neglect of trapping is not entirely justified. However, the inclusion of trapping effects requires an approach radically different to the one presented in this paper (Kotschenreuther *et al.* 1988, 1992).

Acknowledgments

The author is grateful to Professor R. Singh for fruitful and constructive discussions. The author was supported a Natural Sciences and Engineering Research Council of Canada (NSERC) Research Grant.

* The 'standard' model for the DTEM due to Kadomtsev and Pogutse (1969) is valid for cold ions, $\tau \mapsto 0$.

References

Abramowitz, M., and Stegun, I. (1983). 'Handbook of Mathematical Functions' (Dover: New York).

Antonsen, T. M., and Lane, J. B. (1980). *Phys. Fluids* **23**, 1205.

Antonsen, T., Coppi, B., and Englade, R. (1979). *Nucl. Fusion* **19**, 641.

Artun, M., and Tang, W. M. (1992). *Phys. Fluids* **4**, 1102.

Bhattacharjee, A., Sedlak, J. E., Similon, P. L., Rosenbluth, M. N., and Ross, D. W. (1983). *Phys. Fluids* **26**, 880.

Biglari, H., Diamond, P. H., and Rosenbluth, M. N. (1989). *Phys. Fluids* **1**, 109.

Boozer, A. H. (1980). *Phys. Fluids* **23**, 904.

Boozer, A. H. (1981). *Phys. Fluids* **24**, 1999.

Boozer, A. H. (1982). *Phys. Fluids* **25**, 520.

Braginskii, S. I. (1965). 'Review of Plasma Physics', Vol. 1 (Consultants Bureau: New York).

Connor, J. W., Hastie, R. J., and Taylor, J. B. (1978). *Phys. Rev. Lett.* **40**, 396.

Connor, J. W., Hastie, R. J., and Taylor, J. B. (1979). *Proc. R. Soc. London* A **365**, 1.

Cooper, W. A. (1988). *Plasma Phys. Controll. Fusion* **30**, 1805.

Coppi, B., and Mazzucato, E. (1971). *Phys. Fluids* **14**, 134.

Coppi, B., Rosenbluth, M. N., and Sagdeev, R. Z. (1967). *Phys. Fluids* **10**, 582.

Dominguez, R. R., and Waltz, R. E. (1988). *Phys. Fluids* **31**, 3147.

Dominguez, N., Carreras, B. A., and Lynch, V. E. (1992). *Phys. Fluids* **4**, 2894.

Dong, J. Q., Horton, W., and Kim, J. Y. (1992). *Phys. Fluids* **4**, 1867.

Dorland, W., and Hammett, G. W. (1993). *Phys. Fluids* **5**, 812.

Drake, J. F., and Antonsen, T. M. (1984). *Phys. Fluids* **27**, 898.

Drake, J. F, Guzdar, P. N., and Dimits, A. (1991). *Phys. Fluids* **3**, 1937.

Frieman, E. A., and Chen, L. (1982). *Phys. Fluids* **25**, 502.

Guzdar, P. N., Chen, L., Tang, W. M., and Rutherford, P. H. (1983). *Phys. Fluids* **26**, 673.

Guzdar, P. N., Drake, J. F., Dimits, A. M., and Hassam, A. B. (1991). *Phys. Fluids* **3**, 1381.

Haeseleer, W. D., Hitchon, W. N. G., Callen, J. D., and Shohet, J. L. (1991). 'Flux Coordinates and Magnetic Field Structure' (Springer: Berlin).

Hamaguchi, S., and Horton, W. (1990). *Phys. Fluids* **2**, 1833.

Hamaguchi, S., and Horton, W. (1992). *Phys. Fluids* **4**, 319.

Hamberger, S. M., Blackwell, B. D., Sharp, L. E., and Shenton, D. B. (1990). *Fusion Tech.* **17**, 123.

Hammett, G. W., and Perkins, F. W. (1990). *Phys. Rev. Lett.* **64**, 3019.

Hassam, A. B., Antonsen, T. M., Drake J. F., and Gudzar, P. N. (1990). *Phys. Fluids* **2**, 1822.

Hedrick, C. L., and Leboeuf, J. N. (1992). *Phys. Fluids* **4**, 3915.

Hirshman, S. P., and Betancourt, O. (1991). *J. Comput. Phys.* **86**, 99.

Hirshman, S. P., and Lee, D. K. (1986). *Comput. Phys. Commun.* **38**, 161.

Hong, B. G., and Horton, W. (1990). *Phys. Fluids* **2**, 978.

Horton, W. (1984). 'Handbook of Plasma Physics', Vol. 2 (Elsevier: Netherlands).

Horton, W. (1989). *Phys. Fluids* **1**, 524.

Horton, W., Estes, R. D., and Biskamp, D. (1980). *Plasma Phys.* **22**, 663.

Jarmen, A., Andersson, P., and Weiland, J. (1987). *Nucl. Fusion* **27**, 941.

Kadomtsev, B. B., and Pogutse, O. P. (1969). *Sov. Phys. Doklady* **14**, 470.

Kadomtsev, B. B., and Pogutse, O. P. (1971). *Nucl. Fusion* **11**, 67.

Kim, Y. B., Diamond, P. H., Biglari, K., and Callen, J. D. (1991). *Phys. Fluids* **3**, 384.

Kotschenreuther, M. (1988). *Bull. Am. Phys. Soc.* **34**, 2107.

Kotschenreuther, M., *et al.* (1992). Proc. IAEA Conf. on Controlled Fusion, Paper IAEA-CN-56/D1–2 (IAEA: Wurzburg, Germany).

Lewandowski, J. L. V. (1997*a*). *Can. J. Phys.* **75**, 891.

Lewandowski, J. L. V. (1997*b*). *Phys. Plasmas* **4**, 4023.

Lewandowski, J. L. V. (1997*c*). *J. Phys. Soc. Japan* **66**, 3831.

Lewandowski, J. L. V. (1998). *Plasma Phys. Controll. Fusion* **40**, 283.

Lewandowski, J. L. V., and Ellem R. M. (1999). *Aust. J. Phys.* **51**, 71.

Lewandowski, J. L. V., and Persson, M. (1995). *Plasma Phys. Controll. Fusion* **37**, 1199.

Lewandowski, J. L. V., and Persson, M. (1996). *Aust. J. Phys.* **49**, 1121.

Lewandowski, J. L. V., and Persson, M. (1999). *Can. J. Phys.*, in press.

Liewer, P. C. (1985). *Nucl. Fusion* **25**, 543.
Manheimer, W. D., and Lashmore-Davies, C. N. (1989). 'MHD and Microinstabilities in Confined Plasma' (Adam Hilger: Bristol).
Nilsson, J., and Weiland, J. (1994). *Nucl. Fusion* **34**, 803.
Nordman, H., Weiland, J., and Jarmen, A. (1990). *Nucl. Fusion* **30**, 983.
Parker, S. E., Dorland, W., Santoro, R. A., Beer, M. A., Liu, Q. P., Lee, W. W., and Hammett, G. W. (1994). *Phys. Plasmas* **1**, 1481.
Persson, M., and Lewandowski, J. L. V. (1997). *Plasma Phys. Controll. Fusion* **39**, 1941.
Persson, M., Lewandowski, J. L. V., and Nordman, H. (1996). *Phys. Plasmas* **2**, 3440.
Press, W. H., Flannery, B. P., Teukolsky, S. A., and Vetterling, W. T. (1983). 'Numerical Recipes in Fortran' (Cambridge University Press).
Pogutse, O. P. (1967). *Sov. Phys. JETP* **25**, 498.
Rewoldt, G., and Tang W. M. (1990). *Phys. Fluids* **2**, 318.
Romanelli, F., and Briguglio, S. (1990). *Phys. Fluids* **2**, 754.
Rudakov, L. I., and Sagdeev, R. Z. (1961). *Sov. Phys. Doklady* **6**, 415.
Rutherford, P. H., and Frieman, E. A. (1968). *Phys. Fluids* **11**, 569.
Shats, M. G., Rudakov, D. L., and Blackwell, B. D. (1998). *Phys. Plasmas* **5**, 2390.
Shukla, P. K. (1990). *Phys. Fluids* **2**, 848.
Tang, W. M., Adam, J. C., and Ross, D. W. (1977). *Phys. Fluids* **20**, 430.
Tang, W. M., Rewoldt, G., and Chen, L. (1986). *Phys. Fluids* **29**, 3715.
Taylor, J. B., and Hastie, R. J. (1968). *Plasma Phys.* **10**, 479.
Waelbroeck, F. L., and Chen, L. (1991). *Phys. Fluids* **3**, 601.
Waltz, R. E. (1988). *Phys. Fluids* **31**, 1962.
Waltz, R. E., and Boozer, A. H. (1993). *Phys. Fluids* **5**, 2201.
Waltz, R. E., Dominguez, R. R., and Hammett, G. W. (1992). *Phys. Fluids* **4**, 3138.
Xu, X. Q., and Rosenbluth, M. N. (1991*a*). *Phys. Fluids* **3**, 627.
Xu, X. Q., and Rosenbluth, M. N. (1991*b*). *Phys. Fluids* **3**, 1807.

Appendix: Normal Mode Analysis and Initial-value Problem

In this Appendix we derive the expression for the growth rate (58) and for the real part of the mode frequency (60). We write the (normalised) fluctuating electrostatic potential $\widetilde{\Phi}$ using an eikonal representation

$$\widetilde{\Phi} \equiv \frac{e\Phi}{T_{\rm e}} = \widehat{\Phi}(\zeta, t) \exp(iS/\epsilon)\,, \tag{A1}$$

where S is the eikonal (which varies on the equilibrium scale length) and $\epsilon \ll 1$ is a smallness parameter. To lowest order, we have $\nabla\widetilde{\Phi} = i\mathbf{k}_\perp\widetilde{\Phi}$ where $\mathbf{k}_\perp = \epsilon^{-1}\nabla S$. For an equilibrium magnetic field of the form $\mathbf{B} = \nabla\alpha \times \nabla\psi$ (where α is the field line label and $2\pi\psi$ is the enclosed poloidal flux), one can choose $S = S(\alpha, \psi)$; then the lowest-order perpendicular wavevector $\mathbf{k}_\perp$ is orthogonal to $\mathbf{B}$. To recover the usual representation of the normal mode analysis, one makes the transformation

$$\widehat{\Phi}(\zeta, t) \mapsto \overline{\Phi}(\zeta) \exp(-i\omega t) \tag{A2}$$

in equation (A1). Here ω is the mode frequency. One can write $\omega = \Re(\omega) + i\Im(\omega) \equiv \omega_{\rm r} + i\gamma$. Here $\Re(x)$ and $\Im(x)$ denotes the real and imaginary parts of x, respectively, while $\omega_{\rm r}$ is the real part of the mode frequency and γ is the (linear) growth rate. Our aim is to determine these quantities from the left-hand side of (A2). We have

$$\widehat{\Phi} = [\Re(\overline{\Phi}) + i\Im(\overline{\Phi})] \exp(-i\omega_{\rm r} t + \gamma t)$$

$$= [\Re(\overline{\Phi}) + i\Im(\overline{\Phi})][\cos(\omega_{\rm r} t) - i \sin(\omega_{\rm r} t)] \exp(\gamma t)\,. \tag{A3}$$

Thus $\Re(\widehat{\Phi}) = A \exp(\gamma t)$ and $\Im(\widehat{\Phi}) = C \exp(\gamma t)$, where $A \equiv \Re(\overline{\phi}) \cos(\omega_{\rm r} t) + \Im(\overline{\phi}) \sin(\omega_{\rm r} t)$ and $C \equiv \Im(\overline{\phi}) \cos(\omega_{\rm r} t) - \Re(\overline{\phi}) \sin(\omega_{\rm r} t)$. Using the above notation, we obtain

$$|\widehat{\Phi}|^2 = \widehat{\Phi}\widehat{\Phi}^{\star}$$

$$= [\Re(\widehat{\Phi})]^2 + [\Im(\widehat{\Phi})]^2$$

$$= \exp(2\gamma t)(A^2 + C^2)$$

$$= \exp(2\gamma t)[\Re(\overline{\phi}) \cos(\omega_{\rm r} t)]^2$$

$$+ [\Im(\overline{\phi}) \sin(\omega_{\rm r} t)]^2 + [\Im(\overline{\phi}) \cos(\omega_{\rm r} t)]^2 + [\Re(\overline{\phi}) \sin(\omega_{\rm r} t)]^2]$$

$$= \exp(2\gamma t)[[\Re(\overline{\phi})]^2 + [\Im(\overline{\phi})]^2]$$

$$= \exp(2\gamma t)|\overline{\phi}|^2\,. \tag{A4}$$

Taking the time derivative of equation (A4), we have

$$2|\widehat{\Phi}| \frac{\partial}{\partial t}\ |\widehat{\Phi}| \mapsto 2\gamma \exp(2\gamma t)|\overline{\phi}|^2$$

$$\frac{1}{|\widehat{\Phi}|}\ \frac{\partial}{\partial t}|\widehat{\Phi}| \mapsto \gamma\,. \tag{A5}$$

Thus the linear growth rate is

$$\gamma = \frac{1}{|\langle\widehat{\Phi}\rangle|}\ \frac{\partial}{\partial t}\ |\langle\widehat{\Phi}\rangle|\,. \tag{A6}$$

In the above equation, $\langle ... \rangle$ denotes an average over the mode extent along the field line

$$\langle F \rangle \equiv \frac{1}{2\zeta_{\rm m}}\ \int_{\zeta_0 - \zeta_{\rm m}}^{\zeta_0 + \zeta_{\rm m}} F(\zeta; \theta_0, \zeta_0) d\zeta\,, \tag{A7}$$

where the set (θ_0, ζ_0) identifies the field line of reference (on a given magnetic surface). We now determine the real part of the mode frequency, $\omega_{\rm r}$. We start from

$$\frac{1}{\widehat{\Phi}}\ \frac{\partial\widehat{\Phi}}{\partial t} = \frac{\widehat{\Phi}^{\star}}{|\widehat{\Phi}|^2}\ \frac{\partial\widehat{\Phi}}{\partial t}\,, \tag{A8}$$

where $\widehat{\Phi}^{\star}$ is the complex conjugate of $\widehat{\Phi}$. It is easy to show that

$$\begin{aligned}\frac{\partial\Re(\widehat{\Phi})}{\partial t} &= \exp(\gamma t)\left(\gamma A + \frac{\partial A}{\partial t}\right)\\ &= \exp(\gamma t)(\gamma A + \omega_{\rm r} C)\end{aligned} \tag{A9}$$

and

$$\begin{aligned}\frac{\partial\Im(\widehat{\Phi})}{\partial t} &= \exp(\gamma t)\left(\gamma C + \frac{\partial C}{\partial t}\right)\\ &= \exp(\gamma t)(\gamma C - \omega_{\rm r} A)\,.\end{aligned} \tag{A10}$$

Now, starting from equations (A8)–(A10), we have the following:

$$\begin{aligned}\frac{1}{\widehat{\Phi}}\ \frac{\partial\widehat{\phi}}{\partial t} &= \left[\frac{\Re(\widehat{\phi}) - i\Im(\widehat{\phi})}{|\widehat{\phi}|^2}\right]\left[\frac{\partial\Re(\widehat{\phi})}{\partial t} + i\frac{\partial\Im(\widehat{\phi})}{\partial t}\right]\\ &= \frac{\Re(\widehat{\phi})}{|\widehat{\phi}|^2}\ \frac{\partial\Re(\widehat{\phi})}{\partial t} + \frac{\Im(\widehat{\phi})}{|\widehat{\phi}|^2}\ \frac{\partial\Im(\widehat{\phi})}{\partial t}\\ &\quad + \frac{i}{|\widehat{\phi}|^2}\left[\Re(\widehat{\phi})\frac{\partial\Im(\widehat{\phi})}{\partial t} - \Im(\widehat{\phi})\frac{\partial\Re(\widehat{\phi})}{\partial t}\right]\\ &= \frac{1}{2|\widehat{\phi}|^2}\ \frac{\partial}{\partial t}([\Re(\widehat{\phi})]^2 + [\Im(\widehat{\phi})]^2)\\ &\quad + \frac{i}{|\widehat{\phi}|^2}\ [A\exp(2\gamma t)(\gamma C - \omega_{\rm r} A) - C\exp(2\gamma t)(\gamma A + \omega_r C)]\\ &= \frac{1}{2|\widehat{\phi}|^2}\ \frac{\partial}{\partial t}|\widehat{\phi}|^2 - \frac{i}{|\widehat{\phi}|^2}\ \omega_{\rm r}(A^2 + C^2)\exp(2\gamma t)\\ &= \frac{1}{2|\widehat{\phi}|^2}\ \frac{\partial}{\partial t}\ |\widehat{\phi}|^2 - i\omega_r\,.\end{aligned} \tag{A11}$$

Therefore the real part of the mode frequency is determined as

$$\omega_r = \Re\left(\frac{i}{\langle\widehat{\phi}\rangle}\ \frac{\partial\langle\widehat{\phi}\rangle}{\partial t}\right). \tag{A12}$$

Alternatively one can also use

$$\omega_{\rm r} = -\Im\left(\frac{1}{\langle\widehat{\phi}\rangle}\ \frac{\partial\langle\widehat{\phi}\rangle}{\partial t}\right). \tag{A13}$$

Manuscript received 18 December 1998, accepted 20 August 1999